Mechanisms underlying the cooperation between loss of epithelial polarity and Notch signaling during neoplastic growth in *Drosophila*

Rémi Logeay[1], Charles Géminard[1], Patrice Lassus[2], Diala Kantar[1], Lisa Héron-Milhavet[1], Bettina Fischer[3], Sarah J. Bray[4], Jacques Colinge[1], and Alexandre Djiane[1]*

[1] IRCM, Inserm, Univ Montpellier, ICM, Montpellier, France

[2] IRCM, Inserm, Univ Montpellier, ICM, CNRS, Montpellier, France

[3] Dept. of Genetics, University of Cambridge, Cambridge, United Kingdom

[4] Dept. of Physiology Development and Neuroscience, University of Cambridge, Cambridge, United Kingdom

*Author for correspondence: IRCM, Inserm U1194
208, rue des Apothicaires
34298 Montpellier, Cedex, France
tel: +33 (0) 467 612 441
email: alexandre.djiane@inserm.fr

KEY WORDS:
Notch signaling, *Drosophila*, epithelial polarity, neoplasia, cell competition

SUMMARY

Aggressive neoplastic growth can be initiated by a limited number of genetic alterations, such as the well-established cooperation between loss of cell architecture and hyperactive signaling pathways. However, our understanding of how these different alterations interact and influence each other remains very incomplete. Using *Drosophila* paradigms of imaginal wing disc epithelial growth, we have monitored the changes in Notch pathway activity according to the polarity status of cells and show that epithelial polarity changes directly impact the transcriptional output of the Notch pathway. Importantly, we show that this Notch pathway redirection is not mediated by a redeployment of Su(H), the Notch dedicated transcription factor, but relies on the cooperation with a combination of oncogenic transcription factors. Our work highlights in particular the role of the stress response CEBPG homologue CG6272/Irbp18 and of its partner Xrp1 suggesting that parts of the cellular competition program might promote neoplastic growth.

INTRODUCTION

In multicellular organisms, cells constantly integrate many stimuli, to adapt their behaviors and responses. How cells achieve this integration is a fundamental question in biology and its disruption underlies many pathologies. Cancer genomes harbor many mutations and understanding how different mutations interact within a given cell is a major goal in cancer research.

Epithelial cells represent the basic unit of many organs. Their apico-basal (A/B) polarity is controlled by the asymmetric segregation of highly conserved protein complexes such as the Scrib/Dlg/Lgl complex (Bilder et al., 2003; Coopman and Djiane, 2016; St Johnston and Ahringer, 2010). The far-reaching effects of A/B polarity is epitomized by the observation that many tumors of epithelial origin exhibit impaired polarity, and that several viral oncoproteins target polarity complexes (Banks et al., 2012; Huang and Muthuswamy, 2010).

Studies in human cell lines and in animal models have also suggested a contributing role of polarity alterations to tumor formation. For instance, mutations in the baso-lateral determinant *SCRIB1* have been shown to control proliferation and invasion in MCF-10A human mammary cells (Cordenonsi et al., 2011). Similarly in *Drosophila*, *scrib*, *dlg* or *lgl* mutations, result in multilayered overgrowth of larval epithelial imaginal discs (Bilder et al., 2003; Bunker et al., 2015). However, this uncontrolled growth is at least partly achieved because larvae exhibiting *scrib* mutations fail to undergo proper metamorphosis and imaginal discs grow for an extended period. Indeed, *scrib* mutant cells actually grow slower than wild-type cells and are eliminated by wild-type neighbors (Cordero et al., 2010; Igaki et al., 2009, 2006; Ohsawa et al., 2011). Interestingly, this is reversed when additional mutations are

64 introduced, such as overexpression of the BTB/POZ chromatin remodelers Abrupt or
65 Chinmo (Doggett et al., 2015; Turkel et al., 2013) or the constitutive activation of
66 signaling pathways (e.g. Ras or Notch), converting *scrib* mutant cells into aggressive,
67 invasive and hyperproliferative cells (Brumby and Richardson, 2003; Pagliarini and
68 Xu, 2003). Similar observations have been reported in mouse, where Notch or Ras
69 activation and *Par3* depletion cooperate to generate aggressive neoplasms in mouse
70 mammary glands (McCaffrey et al., 2012; Xue et al., 2013).

71 The Notch pathway is a highly conserved cell-signaling pathway mis-regulated in
72 several cancers (Ntziachristos et al., 2014; Ranganathan et al., 2011). Upon activation,
73 Notch receptors undergo two proteolytic cleavages to release their intra-cellular
74 domain or NICD, which enters the nucleus, binds to the Notch pathway specific
75 transcription factor CSL (Rbpj in mammals; Suppressor of Hairless, Su(H) in
76 *Drosophila*), and converts it from a repressor to an activator to turn on the
77 transcription of specific target genes (Bray, 2016). These Notch direct target genes
78 differ depending on cell type and account for the variety of outcomes triggered by
79 Notch activity. Increased Notch activity has been associated with several epithelial
80 cancers such as non-small-cell lung carcinomas (Maraver et al., 2012; Ntziachristos et
81 al., 2014), but in animal models, the sole increase in Notch activity either promotes
82 differentiation or only results in benign over-proliferation (hyperplasia) (Brumby and
83 Richardson, 2003; Djiane et al., 2013; Fre et al., 2005; Ho et al., 2015; McCaffrey et
84 al., 2012). However, as mentioned previously, Notch pathway activation cooperates
85 with loss of polarity to generate invasive neoplasms (Brumby and Richardson, 2003;
86 Ho et al., 2015; McCaffrey et al., 2012; Pagliarini and Xu, 2003).

87 So, while the cooperation between loss of cell architecture and hyperactive signaling
88 pathways is well established, the underlying mechanisms remain poorly understood. It

could merely reflect an additive effect where the consequences of both events combine (the additive model). Alternatively, it could indicate a more profound integration within epithelial cells where these two events impact on each other to generate unique new behaviors (the redirective model). Using *Drosophila* paradigms of imaginal wing disc epithelial growth, we have monitored the changes in Notch pathway activity according to the polarity status of cells and show that epithelial polarity changes directly impact the transcriptional output of the Notch pathway. We further provide evidence that this Notch redirection is not mediated by new genomic binding regions for Su(H), but relies on the cooperation with Su(H) of a combination of transcription factors, such as basic leucine zipper (bZIP), whose activity is triggered in response to JNK signaling during polarity loss, extending earlier reports on the cooperation between oncogenic Ras and polarity loss (Atkins et al., 2016; Davie et al., 2015; Külshammer et al., 2015; Uhlirova and Bohmann, 2006). Our work highlights in particular the role of the stress response CEBPG homologue CG6272/Irbp18 and of its partner Xrp1, key factors in mediating the loser fate during cell competition (Baillon et al., 2018; Blanco et al., 2020; Ji et al., 2019; Lee et al., 2018), suggesting that cellular competition, or parts of the cellular competition program, are co-opted during neoplastic growth.

RESULTS

Notch activation and scrib mutation cooperate to promote neoplastic growth

In order to gain insights into the mechanisms underlying neoplastic growth, we first characterized the effects of Notch activation and *scrib* mutation mediated epithelial polarity impairment on wing disc growth. Using precisely controlled *Drosophila* larvae culture conditions (crowding and timing), we compared the phenotypes of wild-type (WT), Nicd overexpressing (N), *scrib* mutant (S), and Nicd overexpressing and *scrib* mutant (NS) 3rd instar wing imaginal discs at 6 days after egg laying at 25C. These different paradigms are shown in Figure 1A-D. For clarity, in all figures N will be shown in green, S in red, and NS in blue. Reproducing our previous observations (Djiane et al., 2013), N discs overgrew compared to WT, but remained as monolayered epithelia with properly localized E-Cadherin-based adherens junctions, and represent a paradigm of hyperplastic-like growth (Fig. 1A&B). S discs were smaller than WT, but grew as unstratified mass of cells with weak uniform E-Cadherin (E-Cad). These discs however showed an extensive expression of the JNK signaling target Mmp1 (Fig. 1C), a metallo-protease implicated in the digestion of the extracellular matrix, indicative that *scrib*- cells activate JNK signaling and are prone to invasiveness (Igaki et al., 2006; Uhlirova and Bohmann, 2006). It is noteworthy that S larvae did not pupariate and if left to grow for longer, the S discs ultimately developed as massive overgrowths with very disrupted epithelial polarity, that invaded and fused with neighboring tissues such as other discs (Bilder et al., 2003). Strikingly, NS discs combined aspects of N and S discs. They were overgrown like N discs, but also expressed low levels of E-Cad and high levels of Mmp1 like S discs (Fig. 1D). These discs grew as multilayered tissues and were able to invade the surrounding tissues such as haltere discs, and represent therefore a paradigm for neoplastic-like growth.

Neoplastic and hyperplastic discs have different transcriptomes

The context of the scribble mutation converts the Notch-based *Drosophila* wing disc into a paradigm of neoplastic growth. Until now, the cooperation between activated Ras and *scrib* mutations has been studied extensively, mainly in the imaginal eye disc (Atkins et al., 2016; Cordero et al., 2010; Davie et al., 2015; Igaki et al., 2009; Katheder et al., 2017; Pagliarini and Xu, 2003; Toggweiler et al., 2016; Wu et al.,

2010), but less attention has been given to the way that other activated pathways, such as Notch or Hedgehog, also cooperate with polarity loss beyond the initial studies (Brumby and Richardson, 2003; Pagliarini and Xu, 2003). Exploring how these other pathways cooperate is important to evaluate the extent that are generally important for neoplasia or specific to Ras signaling induced transformations.

First, we compared the transcriptomes of the different genetic conditions, to identify genes whose expression was significantly different. Differential expression analyses of genome-wide RNA-seq profiles (using DESeq with adjusted p-value for multiple testing <0.05; (Anders and Huber, 2010) identified the cohorts of genes that were significantly up-regulated or down-regulated in each condition compared to WT controls (Fig. 1E&F and Supplemental Tables 1-3). The numbers were broadly similar in each condition N (503 up; 663 dw), S (757 up; 1029 dw), and NS (1003 up; 991 dw). Using semi-quantitative qRT-PCR we then validated a subset of the transcriptional changes and could confirm the specific differences. The N only affected genes *E2f1*, *Sdr*, and *mxc*, were activated only in N discs and not in S or NS while the S only gene *p38a* and the NS only genes *Act87E* and *Wnt10*, were activated only in their respective conditions. In addition, *Ets21C*, *ftz-f1*, and *Atf3* were up-regulated in all three conditions, as detected by the RNA-Seq profiles (Fig. 1G) Comparing these data with previously published transcriptome analyses on similar or related genetic backgrounds revealed significant overlap, validating our experimental approaches. For instance, 174 of the 503 up-regulated genes in N, and 285 of the 663 down-regulated genes were also detected in our previous analysis using dual color differential expression arrays (significant overlap p=1.11e-273, hypergeometric test, (Djiane et al., 2013). Similarly, 676 of the 757 up-regulated genes in S were identified in a previous analysis of *scrib* depleted discs (significant overlap p=4.90e-193; (Bunker et al., 2015).

To gain insights into the nature of the mis-regulated genes we performed a GO term analysis on the genes affected in N, S, and NS (p-value < 0.05). As expected from their genetic composition, the N and NS tissues were over-represented for genes in the Notch signaling pathway (GO:0007219) and the NS and S had changes in A/B polarity (GO:0045197; GO0019991) (Fig. 2A and Supplemental Tables 4&5). Focusing on the other most robust GO terms (q-value < 0.05) revealed common

alterations in all three growth paradigms which included cell adhesive properties (GO:0030198 “extracellular matrix organization”; GO:0007155 “cell adhesion”), ribosomal biology (GO:0042274/GO:0042273 “ribosomal small/large subunit biogenesis”) suggesting that protein synthesis might be affected, mis-regulated metabolic processes, in particular with respect to glucose and glycolysis (GO:0006002), or oxidative stress (GO:0006979 “response to oxidative stress”; Fig. 2A and Supplemental Tables S4&5).

Despite these similarities, there were also differences in the profiles. For example, markers of increased proliferation were found in both NS and N, but not S, consistent with the overgrowth phenotypes (e.g. “mitotic cytokinesis” and “mitotic spindle organization”; GO:0000281; GO:0007052). The overgrowing behavior of NS tissues may therefore be driven by the Notch activation (Fig. 2A and Supplemental Tables S4&5) although it should be noted that N was enriched in additional mitosis related categories such as “mitotic metaphase plate congression” or “centriole replication” (GO:0007080; GO:0007099), suggesting a more robust proliferation signature in N tissues. Similarly, both NS and S (but not N) showed characteristics of cell migration (e.g. “border follicle cell migration”; GO:0007298) and cellular stress such as “response to starvation” (GO:0042594), or “response to endoplasmic reticulum stress” (GO:0034976) suggesting that these features in NS were likely contributed by the *scrib* mutation (Fig. 2A and Supplemental Tables S4&5).

Notably there were several GO categories specific to NS including “positive regulation of apoptotic signaling pathway” (GO:2001235) “negative regulation of SAPK signaling cascade” (GO:0070303) and “mitotic G1/G2 DNA damage checkpoint” (GO:0031571/GO:0007095). These results argue that the combined Notch activation and polarity loss promoted the emergence of new cell behaviors and responses, in particular related to DNA damage responses (Fig. 2A&B and Supplemental Tables S4&5).

Distinguishing between the additive and redirective models of cooperation

The transcriptomic changes revealed that NS encompassed not only additive N and S features but also the emergence of new behaviors. This raises the question of how the defects in *Notch* and in *scrib* cooperate to produce these transcriptional consequences.

Two main models could be proposed for genetic cooperation: (1) an additive model, in which the effect of each genetic change is independent and summed to produce the phenotype, and (2) a redirective model, in which the two mutations influence each other to change their effects. Since Notch signaling exerts a direct effect on transcription, without intermediates (unlike Ras and RTK signaling for instance; (Bray, 2016), our Notch-based paradigms may allow us to distinguish between the two models. Indeed, in the N and NS paradigms overexpressing the transcriptional activator Nicd, the genes directly activated by Notch (Notch Direct Targets, NDTs), should behave differently depending on whether the cooperation is additive or redirective. In the additive model, genes directly activated by Notch should be insensitive to the polarity status of the cells and should remain the same in the hyperplastic (Nicd only) and neoplastic (Nicd & *scrib*-). Alternatively, if the loss of polarity affects Notch directly, the directly activated genes should be, at least in part, different.

Genes that are directly regulated by Notch (NDTs) should have the transcription complex, containing Su(H) bound at their regulatory regions (Djiane et al., 2013). To identify potential NDTs in N and NS, we thus monitored the genomic regions occupied by the Su(H) transcription factor by genome-wide Chromatin Immuno-Precipitation (ChIP) (Supplemental Table S6). These overlapped significantly with our previous analysis of Notch induced overgrowth, suggesting that we have captured all the robust regions of Su(H) enrichment.

Strikingly, there was a strong overlap in the Su(H) bound regions in both conditions: almost all (416 out of a total of 464) NS Su(H) peaks overlap with peaks present in N discs. This implies that the vast majority of Su(H) binding remained the same in N and NS (Fig. 3C & S1C). The overlap was also important between N and S peaks (447/554 S peaks overlapping with N peaks; Fig. 3C & S1C). These results suggests that in NS neoplastic discs (and to a lesser extent in S discs), a minority of Su(H) peaks represent new binding regions compared to hyperplastic N discs, and that the new NS behaviors are not the consequence of general redistribution of the Notch specific transcription factor Su(H).

We note that the majority of binding in all conditions is associated with intronic regions (39.70% and 42.89% in N and NS respectively; Fig. S1A), which are

frequently the site of enhancers in *Drosophila* patterning and growth genes. There was a subtle shift in the distribution in other regions with a decrease in Su(H) peaks that were associated with promoter regions in NS discs (from 31.55% in N to 23.06% in NS; Fig. S1A) complemented by an increase in Su(H) binding associated with intergenic regions (from 15.51% in N to 20.47% in NS; Fig. S1A), but the significance of this shift is unclear.

In order to estimate the programs specifically activated by Notch in N, S, and NS, we then intersected the transcriptomic data with the Su(H) ChIP data, considering that upregulated genes located within 20kb of a Su(H) peak were likely NDTs. Using this approach, we identified similar numbers of NDTs in N (177) and NS (171) (Fig. 3A&B, Supplemental Table S7). Again, there was substantial overlap with previous data, with 64/177 NDTs in N conditions being identified in our previous study (significant overlap p=5.89e-96, hypergeometric test (Djiane et al., 2013). When the N and NS scenarios were compared, 69 genes were common to both and thus represent core NDTs in the wing disc overgrowth. However, a significant proportion of NDTs appeared specific for each condition: 108 for N, 102 for NS (Fig. 3B) which supports the redirective model. Amongst the 102 NS-specific NDTs, only 24 were also NDTs in S, arguing that the difference cannot be explained by specific contribution of the S condition. Taking all of these comparisons into account, there appear to be 78 genes that are NS-specific NDTs. Only a minority were associated with new Su(H) binding regions: around the *87E* locus (*yellow-e3*, *yellow-e*, *Ir87a*, and *Act87E*), and the *94A* locus (*CG18596*, *CG7059*, *CG13857*, and *CG13850*). Amongst these 78 NS specific NDTs are p53, His2Av, and the Tip60 complex component Act87E (Kusch et al., 2004), which have all been linked to DNA damage response and could therefore account for the NS emergent behaviors identified in the GO term analysis (Fig. 2A and Supplemental Tables S4&5). The Venn-diagrams representing the overlaps in N, S, and NS, highlight the extent of additivity (the yellow circles encompassing common NDTs) and the scale that there is redirection of the Notch pathway output (red circles). Both losses and gains occur so that in the conditions where there is neoplastic growth (NS), 78 new NDTs are acquired while 108 NDTs are no longer present compared to N (and 70 compared to S). The observation that the NDTs differ substantially between NS and N is in strong support of the redirective model.

Taken together, our results indicate that Notch activation and *scrib* mediated loss of polarity cooperate both in an additive and redirective manner to promote neoplastic growth, and that the redirection of the Notch pathway transcriptional output is not a consequence of a general redeployment of Su(H) to new active sites. They argue that alterations in the cell architecture can directly influence the outcome of the Notch signaling pathway and support a model in which different genetic injuries within tumor cells could thus influence each other to sustain neoplastic growth.

Identification of the transcriptional networks in our different growth paradigms

Using the NDT datasets, we sought to identify the factors that are required for the transition from N hyperplastic to NS neoplastic growth. As the NS transcriptome showed signatures consistent with "response to oxidative stress" (GO:0006979), "cellular response to gamma radiation" (GO:0071480), and "DNA damage checkpoints" (GO:0031571/0007095), we first asked whether interfering with such pathways could block the growth and invasiveness of NS tissues.

To perform these genetic tests, we generated a stable fly line which overexpressed *Nicd* and *scribRNAi* together with a *GFP* marker under the *BxGal4* driver (driving expression in the pouch of the larval wing discs; *Bx>NS*), and monitored the size of the overgrowth (GFP positive tissue), and its invasiveness potential (Mmp1 expressing cells; Fig. 5A). Blocking the oxidative stress response by overexpressing the Reactive Oxygen Species (ROS) sponge CAT and SOD, or knocking down by RNAi the expression of *ATM* or *ATR* (*tefu* or *mei-P26* in the fly), the two master kinases mediating the early response to DNA damage (double or single strand breaks respectively) did not have any significant effect on the NS overgrowth or the expression of Mmp1 (Fig. 5I). Similarly, expression of RNAi or dominant negative forms of the acute stress response and severe DNA damage major effector and NS specific NDT *p53* could not modify the NS overgrowth phenotype (Fig. 5I). While we cannot exclude that the tools used here were not strong enough, these results suggest that even though activated in NS tissues, oxidative stress and DNA damage responses were either not required to sustain NS growth, or that they could compensate for each

other converging ultimately on an as yet unidentified core response promoting NS growth.

Next we sought to identify transcriptional factors that could account for the cooperation between Notch and polarity loss. We used the iRegulon software to identify the transcriptional network involved. When utilized to analyze genes involved in sustaining the tumorous growth of *RasV12/scrib*- 3rd instar larval eye, wing and leg discs, it highlighted the role of the Hippo pathway terminal effectors Yki/Sd and their targets Myc, Crp, and Ftz-F1, the JNK pathway regulated AP-1 factors (in particular Atf3, Kay, and CEBPG), and the Jak/Stat pathway (Atkins et al., 2016; Davie et al., 2015; Külshammer et al., 2015).

Implementing iRegulon on our step-wise Notch-based paradigms allowed us (i) to identify transcriptional modules unique or shared between polarity loss only (S), proliferation only (N) and proliferation plus invasiveness (NS), and (ii) to assess the conservation of the "oncogenic" modules identified previously with Ras in a Notch-driven neoplastic paradigm. We performed these analyses feeding iRegulon either with the lists of up-regulated genes in N, S, and NS (Fig. 4A & Supplemental Tables S7-11) or with the lists of NDTs (Fig. S2 & Supplemental Table S12-15). We decided to focus our analyses on the up-regulated genes here since: i) the overexpressed Nicd triggers transcriptional activation (Bray, 2016) and down-regulated genes might thus represent very indirect effects of the cooperation, and ii) the Su(H) module should be found enriched in the regulatory regions of the up-regulated genes and represent thus an internal control to evaluate the bio-informatic predictions. These analyses identified "modules of transcription factors" likely co-regulating the genes identified in N, S, or NS. Modules identified are presented as Venn diagram (Fig. 4A & S4) to highlight common and specific programs in the different conditions. Feeding either up-regulated genes (Fig. 4A) or NDTs (Fig. S2) identified similar modules indicating that the Notch pathway redirection is mediated, at least in part, by transcription factors that broadly affect the whole transcriptome. This is likely also true for other neoplastic paradigms such as Ras, even though this remains to be established. Importantly, iRegulon identified the Notch pathway dedicated transcription factor Su(H) in the N and NS transcriptomes.

First, focusing on NS, which most resembles the *RasV12/scrib-* paradigms, our analysis identified the same major nodes and oncogenic module as described previously:

- AP-1 basic Leucine Zipper factors related to stress kinase signaling; *Mmp1* is a canonical JNK targets and is highly expressed in NS growing discs (Fig. 1D)
- Stat92E of the Jak/Stat pathway; *upd3* coding for the upstream ligand of the Jak/Stat pathway is indeed highly expressed in NS discs
- Ftz-F1 nuclear receptor
- basic Helix-Loop-Helix factors of the Myc family.

In NS transcriptome, we also identified a contribution of the E(spl) bHLH transcriptional repressors. E(spl)-HLH genes are canonical Notch targets, and they are robustly up-regulated in N and NS, in particular E(spl)mγ-HLH. In NS there were however two noteworthy differences when focusing only on NDTs, rather than all differentially transcribed genes. (1) The absence of the E(spl) factors, suggesting that when considering the whole NS transcriptomes a significant of genes could be associated with E(spl)-mediated regulation while this is no longer the case when considering the more restricted number of NS NDTs. (2) The identification of Ewg, the fly NRF1 homologue. In mammals, NRF1 is implicated in the regulation of key metabolic and respiratory genes (Herzig et al., 2000).

The iRegulon analyses also suggested that the AP-1 bZIP, and the Stat92E signatures in NS are contributed by S, since they are also detected in the S transcriptomes, while the Su(H) signature is contributed by N. Interestingly, the bHLH Myc signature is found in N and S as well as NS. Finally, iRegulon identified a signature for the Polycomb chromatin silencers specifically in N. Such factors include Pho, a zinc finger protein which binds to Polycomb Responsive Elements (PREs) and recruits Polycomb complexes, and the three Polycomb Repressor Complex 1 components Psc, Su(z)2, and l(3)73Ah. Recently, PRC1 has been associated with specific and unexpected transcriptional activation at larval stages, raising the possibility that in N, such genes, normally repressed at embryonic stages, become active (Loubiere et al., 2020).

A polarity-loss oncogenic module

In order to validate the functional relevance of the transcription factors identified in the Notch-driven neoplastic growth, we then asked whether their depletion by RNAi could alter the growth and invasiveness of the NS tissue, using the *Bx>NS* fly line described previously. We first focused our analysis on the the oncogenic module.

We confirmed earlier reports that blocking JNK activity by the overexpression of a JNK dominant negative construct, strongly abolishes NS driven growth (GFP positive tissue size; Fig. 5B&J) and invasiveness (Mmp1 expression; Fig. 5B&J'). As shown in the *RasV12/scrib-* paradigms, RNAi mediated knock-down of the Jak/Stat pathway terminal transcription factor *stat92E*, the JNK pathway component *Ets21C*, and to a lesser extent *ftz-f1* (Atkins et al., 2016; Davie et al., 2015; Külshammer et al., 2015; Toggweiler et al., 2016) strongly suppressed both growth (GFP) and invasiveness (Mmp1; Fig. 5J&J'). Unlike the RasV12 models, we did not identify any particular enrichment for Sd/TEAD, the transcriptional factor mediating the effect of Yki and of the Hippo pathway mediated growth in wing discs. However, impairing Yki activity (through RNAi-mediated knock-down) strongly suppressed NS neoplastic behaviors (Fig. 5C&J).

Taken together these results suggest that independently of the oncogenic driver, Ras or Notch, relatively similar tumorous transcriptional networks (AP-1/Yki/Stat/Ftz-f1) are put in place during their cooperation with polarity loss (Atkins et al., 2016; Davie et al., 2015; Külshammer et al., 2015). Given that these nodes were also identified in the S transcriptome, we suggest that they might represent a polarity loss module cooperating with oncogenic signaling pathways Ras or Notch (and likely other pathways such as Hh as was initially reported; (Brumby and Richardson, 2003).

The CG6272/Xrp1 module is required for neoplastic growth

A striking feature of the iRegulon analyses was that the JNK module, which contained classic basic leucine zipper (bZIP) transcription factors such as Jun or Fos, was found in NS and S. As the bZIP factors identified belonged to sub-families involved in different cellular responses including oxidative stress (Maf-S, Cnc, (Sykiotis and Bohmann, 2008), polarity loss (Atf3, (Donohoe et al., 2018), ER stress (Atf6, Crc, (Harding et al., 2003; Ye et al., 2000), DNA damage… they were potential candidates to mediate the transcriptional switch. First, we analyzed whether these

different bZIP factors were specifically up-regulated in NS (Fig. 4B). Most factors, with the exception were upregulated in S, suggesting that polarity impairment promotes the expression of many bZIP factors which could alter the response of the transcriptional machinery. A further up-regulation in NS, even compared to S, could be detected for kay, crc, maf-S, CG7786, and CrebB (Fig. 4B). Strikingly, cnc and Xrp1were upregulated only in NS (Fig. 4B). It should be noted however, that gene up-regulations do not always indicate functional relevance. Then, in order to identify which bZIP factor/family is most relevant for NS, we therefore systematically depleted by RNAi the different genes highlighted by iRegulon in this bZIP node, irrespective of their potential up-regulations in NS, using the *Bx>NS* fly line.

Amongst the different factors tested, we observed a significant suppression of the invasiveness (Mmp1; Fig. 5K') but not of the growth (GFP; Fig. 5K) of NS tissues after impairing the AP-1 factors *kay* and *Jra* (fly homologues of *FOS* and *JUN* respectively), and *CrebB-17A*. Conversely, knocking down the DNA damage response factor *maf-S* led to a dramatic reduction of the GFP outgrowth but without affecting the invasiveness in which the tissue was expressing high levels of Mmp1 (Fig. 5G&K). It should be noted here that these *maf-S* depleted discs appeared sick with a severely irregular and misshapen GFP domain (Fig. 5G&K, star), suggesting that maf-S might be an essential gene, and that the size suppression might merely reflect enhanced cell death. In contrast, we did not observe any significant effect when *cnc*, the fly homologue of *NFE2L1* implicated in oxidative stress response and excision repair (Han et al., 2012; Sykiotis and Bohmann, 2008), *Atf2*, *gt*, *CG7786*, *vri* (Fig. 5K), were knocked-down. Neither were any consequences on the phenotype with knock-down of *Atf6* and *crc* (the *ATF4* fly homologue), which have been both linked to the unfolded protein response and ER stress (Fig. 5D&K; (Harding et al., 2003; Ye et al., 2000).

The most complete suppression of the NS behaviors (both GFP overgrowth and Mmp1 invasiveness) was observed after depletion of *Atf3*, *Pdp1* or CG6272 (Fig. 5E,H,K). Atf3 has recently been shown to control the expression of genes involved in the maintenance of epithelial polarity, and to be specifically activated in polarity deficient cells and required in the RasV12/scrib- overgrowth models (Atkins et al., 2016; Donohoe et al., 2018). Pdp1 (the homologue of Hepatic Leukemia Factor -

HLF) has previously been linked to mitotic cell cycle and growth (Reddy et al., 2006), and shown in the *RasV12/scrib*- paradigms to have modest effects on invasion, but none on growth. The role of *CG6272* (a.k.a. *Irbp18*, the homologue of *CEBPG*) was also highlighted in the *RasV12/scrib*- paradigms where it was shown to control growth but not invasion (Atkins et al., 2016). In the context of Notch (*Nicd/scrib*-), the role of *Pdp1* and *CG6272* appeared more essential.

bZIP factors have been shown to act as homo or heterodimers. Knocking down the function of *crc/Atf4*, the classic bZIP partner of CG6272/CEBPG, did not have any effect on NS tissue behaviors (Fig. 5D,E,K) whereas the knock-down of *Xrp1* very efficiently suppressed the growth and Mmp1 expression in NS tissues. This suggests that .CG6272/CEBPG could be acting in combination with its bZIP partner Xrp1 in this context (Francis et al., 2016; Reinke et al., 2013). Although the cellular processes controlled by CG6272/Xrp1 remain to be determined, the fact that Xrp1 is an early p53 target gene (Akdemir et al., 2007; Link et al., 2013), raises the possibility that its functions could be related to DNA/genome integrity maintenance. This would align with the NS specific GO categories “cellular response to gamma radiation” (GO:0071480), and “DNA damage checkpoints” (GO:0031571/0007095). Indeed, Xrp1 has recently been linked to cell competition and shown to control the expression of a subset of genes activated in response to Ribosomal protein haplo-insufficiency including *Ets21C*, *upd3*, or *ilp8* in developing wing discs (Baillon et al., 2018; Boulan et al., 2019; Ji et al., 2019; Lee et al., 2018). Strikingly, we observed a very strong overlap between the Xrp1 transcriptional program (Supplemental Table S16) and the genes activated in NS (60 out of the 171 Xrp1 positively regulated genes are also upregulated in NS; hypergeometric test, p=4.71 10e-21), while a much more modest overlap could be observed with N or S (overlap of 17 and 33 with p values of 1.12 10e-3 and 1.56 10e-8 respectively). These results support the proposal that the CG6272/Xrp1 module is functionally important in the acquisition of neoplastic growth.

DISCUSSION

In this study, using Notch-driven paradigms of epithelial overgrowth in *Drosophila* wing discs, we describe the molecular mechanisms underlying the cooperation between Notch and polarity loss during neoplasia. We show that epithelial polarity alterations redirect the transcriptional outcome of the Notch signaling pathway. We further show that this redirection occurs mainly on pre-existing Su(H) bound regions rather than new ones. Finally, we show that similarly to what was previously described for Ras signaling (Atkins et al., 2016; Davie et al., 2015), the cooperation between Notch signaling and polarity loss is controlled by a "tumor transcriptional network" centered around the AP-1/Stat/Yki transcription factors, and including the critical bZIP factors Pdp1 and CEPBG (CG6272/Irbp18). But our analysis uncovered a previously unreported role for the cell competition regulator, and Irbp18 binding partner Xrp1 (Baillon et al., 2018; Blanco et al., 2020; Boulan et al., 2019; Ji et al., 2019; Lee et al., 2018), raising the interesting prospect that neoplastic growth could be mediated at least in part, by co-opting cell competition.

While cancer genomes exhibit multiple mutations in cancer cells, their functional interactions remain difficult to monitor and model. This analysis in the genetically controlled *Drosophila* wing disc, supports a model in which the effects of different mutations do not just simply add up, but interact with each other leading to the emergence of new cell behaviors (redirective model). Indeed, even though the combination showed characteristics that could be attributed to either Notch (proliferation and mitosis), or to polarity loss (invasion/cell migration), it also exerted signs of emerging behaviors such as DNA damage response. Neoplastic tissues appear thus to experience many cellular stresses: DNA damage responses, but also ER and unfolded protein response, starvation, or oxidative stresses. However, even though present, these different stresses and in particular oxidative stress and DNA damage are not individualy necessary in the context of polarity loss as blocking them or the cellular response they promote (CAT/SOD overexpression, or inhibition of ATM/ATR) could not significantly suppress the NS tumorous behaviors. These observations suggest that the different stress pathways activated during polarity loss might all converge leading ultimately to the activation of a common core response.

While *Drosophila* and mouse models have demonstrated that overactive signaling pathways cooperate with epithelial polarity impairment to generate neoplastic growth (Brumby and Richardson, 2003; McCaffrey et al., 2012; Pagliarini and Xu, 2003; Xue et al., 2013), the vast majority of studies seeking to understand the underlying mechanisms, have focused primarily on the cooperation between activated RasV12 and *scrib* mutants, especially in *Drosophila* (Atkins et al., 2016; Cordero et al., 2010; Davie et al., 2015; Igaki et al., 2009; Katheder et al., 2017; Pagliarini and Xu, 2003; Toggweiler et al., 2016; Wu et al., 2010). Importantly, the current study, investigating the cooperation between Notch and polarity, shows that many observations made for Ras can be extended to Notch, suggesting that the paradigms used are not a Ras specificity but might represent a more general tumor growth paradigm.

But even though we could highlight the involvement of a core "oncogenic module" (Atkins et al., 2016; Davie et al., 2015; Külshammer et al., 2015), there are specifics that are likely oncogene specific. In the case of Ras, it was shown that Yki activity could reprogram Ras by promoting the expression of the Ras pathway specific regulators Capicua and Pointed to promote aggressive growth (Pascual et al., 2017). Both genes were either unaffected (*capicua*) or downregulated (*pointed*) in NS Notch driven neoplastic paradigm, suggesting that, even though Yki is clearly active (Fig. 5C), changes in the expression of capicua and pointed are unlikely mediators here. Furthermore, in NS transcriptome, we identified a contribution of the E(spl) bHLH transcriptional repressors, canonical Notch targets (Bray, 2016), which represents thus a Notch specificity. However, the fact that motifs for E(spl)-HLH repressors are found in the up-regulated transcriptome of NS and not N could suggest that in NS, the repressive ability of E(spl)-HLH factors is antagonized (even though their expression is not affected). It would be interesting to explore further the link between NS and E(spl)-HLH-mediated repression, but due to the high redundancy between the seven E(spl)-HLH factors (δ, γ, β, 3, 5, 7, 8) and Dpn, the requirement of E(spl)-HLH-mediated repression in the Notch-driven neoplasia could not be formally tested.

Amongst the most dramatic suppressors of the neoplastic growth are the two basic leucine zipper transcription factors CG6272/Irbp18 (the fly homologue of CEBPG), and Xrp1. These two genes, and in particular *Xrp1*, were up-regulated in NS

compared to WT or N. Importantly, impairing with their function in wild-type tissues did not have any effect, confirming observations made by other groups for CG6272 (Atkins et al., 2016), supporting a model in which these genes are dispensable in healthy wild-type cells, but become indispensable for tumor cells, hence representing a possible attack strategy specifically targeting tumor cells, while sparing healthy tissues. In mammals, CEBPG represents a major regulator of stress responses. It is recruited through its interaction with the bZIP factor ATF4 at the level of cis-regulatory C/EBP:ATF response elements to activate the expression of stress mitigation genes such as glutathione biosynthesis pathway genes in the case of oxidative stress (Huggins et al., 2015). Interestingly, we did not observe any effect knocking down *Crc*, the fly *Atf4* homologue, suggesting that during NS overgrowth in *Drosophila*, CG6272/Irbp18 could be acting in combination with another partner. CG6272/Irbp18 also interacts with Xrp1, and the heterodimer has been implicated in DNA repair (Akdemir et al., 2007; Francis et al., 2016). We thus propose that the Irbp18/Xrp1 dimer is activated in NS and is required to facilitate DNA repair and ensure genomic stability to prevent catastrophic genotoxic effect upon the combined cellular stresses of S and replication stress of N. Recently, *Xrp1* together with its binding partner CG6272/Irbp18 (but not Atf4) has been shown to mediate a loser status in ribosomal genes deficient cells, through the implementation of a specific transcriptional program (Baillon et al., 2018; Blanco et al., 2020; Ji et al., 2019; Lee et al., 2018). This “loser state” promoter role of Xrp1/Irbp18 is however in conflict with our observation that *Xrp1* is strongly upregulated in NS overgrowing discs, and that *Xrp1* and *Irbp18* are required for the overgrowth and invasive capacities of NS neoplastic cells. This could be reconciled by proposing that in NS neoplastic discs, the role of the Xrp1/Irbp18 is modified by an as yet unknown factor. Alternatively, and more attractively, it is also possible that in NS cells, cell death is prevented as was shown for RasV12 expressing cells (Pinal et al., 2018), for instance by upregulating DIAP1 (a Notch direct target, (Djiane et al., 2013) leading to a perverted cell competition. There an incomplete “loser” program would be initiated, but not fully implemented (no cell death), leading to the secretion of growth factors (e.g. the Jak/Stat ligands upd…) that would act in an autocrine manner to further promote their growth. These factors do not actually need to act cell autonomously, since it was shown that at least in the *RasV12 / scrib*- paradigm, delaminating cells cooperate with non-delaminating proliferating cells to sustain tumor growth (Muzzopappa et al.,

2017; Uhlirova et al., 2005; Wu et al., 2010). In NS, preventing the losing/delaminating cells by impairing the Xrp1/Irbp18 nexus, would thus prevent neoplastic growth. This intriguing possibility highlights that more studies are needed to better understand the role of the Xrp1/Irbp18 module, its links to cell competition, and to the growth of neoplastic tissues.

MATERIALS AND METHODS

Drosophila genetics

The different overgrowth paradigms were obtained by generating random clones in 3rd instar wing discs at high frequency as previously published in (Djiane et al., 2013). In brief, the *abxUbxFLPase; Act>y>Gal4, UAS GFP; FRT82B tubGal80* flies were crossed either to *FRT82B* (to generate Ctrl discs), or to *UAS-Nicd; FRT82B* (to generate hyperplastic N discs), or to *UAS-Nicd; FRT82B scrib1* (to generate neoplastic NS discs). *scrib1* represents a loss of function allele for the *scribble* gene. Because *scrib1* clones are eliminated in growing discs, the dysplasic S discs were obtained from *FRT82B scrib1 / Df(3R)BSC752* 3rd instar larvae. All crosses were performed at 25°C and carefully staged (time after egg laying and tube crowding). For functional studies, neoplastic growth was obtained by driving *UAS-Nicd* and the *scrib* RNAi *P{TRiP.HMS01490}attP2* by the *Bx-Gal4* (pouch of larval wing discs). Modifications of the overgrowth phenotype and of the expression of the Mmp1 invasive marker were performed by crossing in F1 *Bx-Gal4, UAS GFP;; UAS Nicd, UAS scribHMS01490* to the desired *UAS RNAi* or control lines (*UAS white RNAi* or *UAS GFP*), to ensure similar UAS load. List of lines tested in Supplemental Materials.

Information on gene models and functions, and on *Drosophila* lines available were obtained from FlyBase (flybase.org – (Thurmond et al., 2019).

RNA extraction and RNA-Seq

RNA from 60 or 80 dissected third instar larva wing discs of WT, N, NS and S discs was extracted using TriZOL. Genomic DNA was eliminated using Ambion's DNA-free kit (#AM1906). cDNA bank preparation were then performed from 1µg of RNA and sequencing on a Illumina HisSeq 2000 by the Biocampus genomic facility MGX of Montpellier. After sequencing, reads obtained were filtered based on their quality (circa 40 millions reads were kept per conditions). The reads were then align on *Drosophila* dm6 genome by the ABIC facility in Montpellier producing a matrix of reads per gene and per condition. This matrix was then normalized and pair-wise differential expression was performed using DESeq (Anders and Huber, 2010). Other differential expression tools were tested such as DESeq2 and edgeR with default parameters but appeared either less stringent, or inadequate.

qPCR

qPCR was performed on biological triplicates on a Roche LightCycler 480, and fold change was estimated by the δδCT approach. List of primers used in Supplemental Materials.

Su(H) Chromatin Immuno Precipitation

After dissection in PBS 1X, Protein/DNA complexes from 60 wing discs (80 for S condition) were cross-linked with 1% formaldehyde for 10 minutes. The reaction was then quenched by 0.125 M Glycine and washed 3x in PBS. Wing disc cells were resuspended in 50µL Nuclear Lysis Buffer (Tris-HCl pH 8.1 20mM, EDTA 10mM, SDS 1%). Lysates were sonicated on a Bioruptor (Diagenode), and diluted 10x in Immunoprecipitation Dilution Buffer (Tris-HCl pH 8.1 20mM, EDTA 2mM, SDS 0.01%, NaCl 150mM, Triton X-100 1%) and precleared with rabbit IgG (Sigma) and protein G Agarose (Santa Cruz Biotechnology). ChIP reactions were performed by incubating lysates overnight at 4°C with 1ng of Goat anti-Su(H) (Santa Cruz Biotechnology, sc15813), and immunocomplexes were then isolated with Protein G Agarose for 2h, washed 2x with Wash Buffer 1 (Tris-HCl pH 8.1 20mM, EDTA 2mM, SDS 0.1%, NaCl 50mM, Triton X-100 1%) and 2x with Wash Buffer 2 (Tris-HCl pH 8.1 10mM, EDTA 1mM, LiCl 250mM, NP-40 1%, Deoxycholic acid 0.4%), before a decross-linking step at 65°C in 0.25M NaCl. Samples were then treated with 0.2 mg/mL proteinase K and 50mg/mL RNase A. The DNA was then purified on columns (Qiagen, 28106). ChIP efficiency was checked by qPCR normalized on input chromatin with the following primer couples, corresponding to known strong binding sites of Su(H). List of primers used in Supplemental Materials.

For whole-genome analysis, 1 µg double-stranded ChIP or input DNA (corresponding to 180 discs for each replicate) was labelled with either Cy3- or Cy5-random primers using the Nimblegen Dual Colour kit. Both ChIP and input were co-hybridised to NimbleGen D. melanogaster ChIP-chip 2.1 M whole-genome tiling arrays in the NimbleGen hybridisation station at 42°C for 16 h and then washed according to the NimbleGen Wash Buffer kit instructions. The data obtained were normalized using quantile normalization across the replicate arrays in R. Window smoothing and peak calling were performed using the Bioconductor package Ringo (Toedling et al., 2007) with a winHalfSize of 300 bp and min.probes = 5. Probe levels were then assigned P-

values based on the normalNull method, corrected for multiple testing using the Hochberg–Benjamini algorithm and then condensed into regions using distCutOff of 200 bp.

In order to determine the Notch Direct Targets (NDTs), ChIP and RNA-Seq results were compared: NDTs are defined as up-regulated genes with Su(H) enrichment within 20kb. As such one Su(H) peak could be assigned to several upregulated genes consistent with its role in enhancer regions. The 20kb window was chosen as it allowed the recovery of more than 85% of NDTs in our previous study that was based on closest gene assignment irrespective of distance (Djiane et al., 2013).

GO Term analyses

The lists of significantly regulated genes in the various comparisons were submitted to gene ontology (GO) term enrichment analysis. We used the GO biological process (GOBP) ontology and applied hypergeometric tests (p-values) followed by Benjamini-Hochberg multiple hypothesis correction (q-values).

iRegulon analyses

In order to determine the likely transcriptional modules in our transcriptomic and NDTs datasets, we used the online tool iRegulon (http://iregulon.aertslab.org/), with the standard settings using the 6K Motif collection (6383 PWMs) and a Putative regulatory region of "10kb upstream, full transcript and 10kb downstream". Importantly, these settings allowed the recovery of the "positive control" Su(H) module.

Immunocytochemistry

Antibody staining of wing imaginal discs were performed using standard protocols. Briefly, larval heads containing the imaginal discs (LH) were dissected in cold PBS and fixed for 20min in 4% Formaldehyde in PBS at room temperature (RT), before being rinsed 3x 10min in PBS 0.2% TritonX100 (PBT), and blocked in PBT + 0.5% BSA (PBTB) for 30min at RT. LH were then incubated overnight at 4°C with primary antibodies in PBTB. LH were then rinsed 3x 10min in PBT at RT and before being incubated with secondary antibody in PBTB for 90min at RT. LH were then rinsed 3x 20min in PBT at RT, before being equilibrated overnight in Citifluor mounting media (Agar). Discs were then further dissected and mounted. Images were acquired on a

Zeiss Apotome2 microscope and processed and quantified using Zen or ImageJ. Primary antibodies used were rat anti-DE-Cadherin (DCAD2, Developmental Studies Hybridoma Bank – DHSB, 1:25), rabbit anti-GFP (A6455, Molecular Probes, 1:200), and mouse anti-Mmp1 (3A6B4, DHSB, 1:25). Secondary antibodies used conjugated to Alexa-350, Alexa-488, or Cy3 were from Jackson Labs Immuno Research (1:200).

Quantification methods

Genotypes were tested in batches with controls and 13-17 images corresponding to 13-17 different discs were all acquired on the same microscope with the same exposure settings.

Growth was estimated by the size of the GFP positive area and normalized to that of controls. A disc was considered overgrown if its size was over the average size of controls plus 1.5 the stdev of controls. A disc was undergrown, if its size was under the average of controls minus 1.5 the stdev of controls. Using this “conservative” set up identified only circa 5% of controls as undergrown.

Mmp1 intensities were ranked as High, Low, Null by independent observer with genotypes masked and processed in random order.

ACKNOWLEDGEMENTS

We thank G. Alvès, D. Andrew, D. Eberl, P. Léopold, R. Levayer, C. Maurange, A. Teleman, J. Terman, and T.T. Su for sharing flies. We acknowledge the Bloomington Stock Center, the Vienna Stock Center, the DGRC Kyoto Stock Center, the Developmental Studies Hybridoma Bank, the *Drosophila* facility, the MGX sequencing facility (BioCampus Montpellier, CNRS, INSERM, Université de Montpellier), and FlyBase for their support to our research.

The lab of SJB is supported by the MRC (MRC programme grant MR/L007177/1). RL was supported by fellowships from “Ligue Nationale Contre le Cancer - LNCC” and from “Fondation ARC pour la recherche sur le cancer”. The lab of AD is supported by the “Fondation ARC pour la recherche sur le cancer”, “Marie Curie CIG”, and “Agence Nationale de la Recherche - ANR”.

AUTHOR CONTRIBUTIONS

RL, CG, PL, DK, and AD performed experiments; RL, CG, LHM, JC, and AD analyzed data; JC provided expertise for RNA-Seq; BF and SJB provided technical support and expertise for ChIP; RL, SJB, and AD wrote the manuscript; AD conceived and supervised the project.

DECLARATION OF INTEREST

The authors declare no competing interests.

REFERENCES

Akdemir F, Christich A, Sogame N, Chapo J, Abrams JM. 2007. p53 directs focused genomic responses in Drosophila. *Oncogene* **26**:5184–5193. doi:10.1038/sj.onc.1210328

Anders S, Huber W. 2010. Differential expression analysis for sequence count data. *Genome Biol* **11**:R106. doi:10.1186/gb-2010-11-10-r106

Atkins M, Potier D, Romanelli L, Jacobs J, Mach J, Hamaratoglu F, Aerts S, Halder G. 2016. An Ectopic Network of Transcription Factors Regulated by Hippo Signaling Drives Growth and Invasion of a Malignant Tumor Model. *Curr Biol* **26**:2101–2113. doi:10.1016/j.cub.2016.06.035

Baillon L, Germani F, Rockel C, Hilchenbach J, Basler K. 2018. Xrp1 is a transcription factor required for cell competition-driven elimination of loser cells. *Sci Rep* **8**:17712. doi:10.1038/s41598-018-36277-4

Banks L, Pim D, Thomas M. 2012. Human tumour viruses and the deregulation of cell polarity in cancer. *Nat Rev Cancer* **12**:877–886. doi:10.1038/nrc3400

Bilder D, Schober M, Perrimon N. 2003. Integrated activity of PDZ protein complexes regulates epithelial polarity. *Nat Cell Biol* **5**:53–58. doi:10.1038/ncb897

Blanco J, Cooper JC, Baker NE. 2020. Roles of C/EBP class bZip proteins in the growth and cell competition of Rp ('Minute') mutants in Drosophila. *Elife* **9**. doi:10.7554/eLife.50535

Boulan L, Andersen D, Colombani J, Boone E, Léopold P. 2019. Inter-Organ Growth Coordination Is Mediated by the Xrp1-Dilp8 Axis in Drosophila. *Dev Cell* **49**:811-818.e4. doi:10.1016/j.devcel.2019.03.016

Bray SJ. 2016. Notch signalling in context. *Nat Rev Mol Cell Biol* **17**:722–735. doi:10.1038/nrm.2016.94

Brumby AM, Richardson HE. 2003. scribble mutants cooperate with oncogenic Ras or Notch to cause neoplastic overgrowth in Drosophila. *EMBO J* **22**:5769–5779. doi:10.1093/emboj/cdg548

Bunker BD, Nellimoottil TT, Boileau RM, Classen AK, Bilder D. 2015. The transcriptional response to tumorigenic polarity loss in Drosophila. *Elife* **4**. doi:10.7554/eLife.03189

Coopman P, Djiane A. 2016. Adherens Junction and E-Cadherin complex regulation by epithelial polarity. *Cell Mol Life Sci* **73**:3535–3553. doi:10.1007/s00018-016-2260-8

Cordenonsi M, Zanconato F, Azzolin L, Forcato M, Rosato A, Frasson C, Inui M, Montagner M, Parenti AR, Poletti A, Daidone MG, Dupont S, Basso G, Bicciato S, Piccolo S. 2011. The Hippo transducer TAZ confers cancer stem cell-related traits on breast cancer cells. *Cell* **147**:759–772. doi:10.1016/j.cell.2011.09.048

Cordero JB, Macagno JP, Stefanatos RK, Strathdee KE, Cagan RL, Vidal M. 2010. Oncogenic Ras diverts a host TNF tumor suppressor activity into tumor promoter. *Dev Cell* **18**:999–1011. doi:10.1016/j.devcel.2010.05.014

Davie K, Jacobs J, Atkins M, Potier D, Christiaens V, Halder G, Aerts S. 2015. Discovery of transcription factors and regulatory regions driving in vivo tumor development by ATAC-seq and FAIRE-seq open chromatin profiling. *PLoS Genet* **11**:e1004994. doi:10.1371/journal.pgen.1004994

Djiane A, Krejci A, Bernard F, Fexova S, Millen K, Bray SJ. 2013. Dissecting the mechanisms of Notch induced hyperplasia. *EMBO J* **32**:60–71. doi:10.1038/emboj.2012.326

Doggett K, Turkel N, Willoughby LF, Ellul J, Murray MJ, Richardson HE, Brumby AM. 2015. BTB-Zinc Finger Oncogenes Are Required for Ras and Notch-Driven Tumorigenesis in Drosophila. *PLoS ONE* **10**:e0132987. doi:10.1371/journal.pone.0132987

775 Donohoe CD, Csordás G, Correia A, Jindra M, Klein C, Habermann B, Uhlirova M. 2018.
776 Atf3 links loss of epithelial polarity to defects in cell differentiation and
777 cytoarchitecture. *PLoS Genet* **14**:e1007241. doi:10.1371/journal.pgen.1007241
778 Francis MJ, Roche S, Cho MJ, Beall E, Min B, Panganiban RP, Rio DC. 2016. Drosophila
779 IRBP bZIP heterodimer binds P-element DNA and affects hybrid dysgenesis. *Proc*
780 *Natl Acad Sci USA* **113**:13003–13008. doi:10.1073/pnas.1613508113
781 Fre S, Huyghe M, Mourikis P, Robine S, Louvard D, Artavanis-Tsakonas S. 2005. Notch
782 signals control the fate of immature progenitor cells in the intestine. *Nature*
783 **435**:964–968. doi:10.1038/nature03589
784 Han W, Ming M, Zhao R, Pi J, Wu C, He Y-Y. 2012. Nrf1 CNC-bZIP protein promotes cell
785 survival and nucleotide excision repair through maintaining glutathione
786 homeostasis. *J Biol Chem* **287**:18788–18795. doi:10.1074/jbc.M112.363614
787 Harding HP, Zhang Y, Zeng H, Novoa I, Lu PD, Calfon M, Sadri N, Yun C, Popko B, Paules R,
788 Stojdl DF, Bell JC, Hettmann T, Leiden JM, Ron D. 2003. An integrated stress
789 response regulates amino acid metabolism and resistance to oxidative stress.
790 *Mol Cell* **11**:619–633. doi:10.1016/s1097-2765(03)00105-9
791 Herzig RP, Andersson U, Scarpulla RC. 2000. Dynein light chain interacts with NRF-1 and
792 EWG, structurally and functionally related transcription factors from humans
793 and drosophila. *J Cell Sci* **113 Pt 23**:4263–4273.
794 Ho DM, Pallavi SK, Artavanis-Tsakonas S. 2015. The Notch-mediated hyperplasia
795 circuitry in Drosophila reveals a Src-JNK signaling axis. *Elife* **4**:e05996.
796 doi:10.7554/eLife.05996
797 Huang L, Muthuswamy SK. 2010. Polarity protein alterations in carcinoma: a focus on
798 emerging roles for polarity regulators. *Curr Opin Genet Dev* **20**:41–50.
799 doi:10.1016/j.gde.2009.12.001
800 Huggins CJ, Mayekar MK, Martin N, Saylor KL, Gonit M, Jailwala P, Kasoji M, Haines DC,
801 Quiñones OA, Johnson PF. 2015. C/EBPγ Is a Critical Regulator of Cellular Stress
802 Response Networks through Heterodimerization with ATF4. *Mol Cell Biol*
803 **36**:693–713. doi:10.1128/MCB.00911-15
804 Igaki T, Pagliarini RA, Xu T. 2006. Loss of cell polarity drives tumor growth and invasion
805 through JNK activation in Drosophila. *Curr Biol* **16**:1139–1146.
806 doi:10.1016/j.cub.2006.04.042
807 Igaki T, Pastor-Pareja JC, Aonuma H, Miura M, Xu T. 2009. Intrinsic tumor suppression
808 and epithelial maintenance by endocytic activation of Eiger/TNF signaling in
809 Drosophila. *Dev Cell* **16**:458–465. doi:10.1016/j.devcel.2009.01.002
810 Ji Z, Kiparaki M, Folgado V, Kumar A, Blanco J, Rimesso G, Chuen J, Liu Y, Zheng D, Baker
811 NE. 2019. Drosophila RpS12 controls translation, growth, and cell competition
812 through Xrp1. *PLoS Genet* **15**:e1008513. doi:10.1371/journal.pgen.1008513
813 Katheder NS, Khezri R, O'Farrell F, Schultz SW, Jain A, Rahman MM, Schink KO,
814 Theodossiou TA, Johansen T, Juhász G, Bilder D, Brech A, Stenmark H, Rusten TE.
815 2017. Microenvironmental autophagy promotes tumour growth. *Nature*
816 **541**:417–420. doi:10.1038/nature20815
817 Külshammer E, Mundorf J, Kilinc M, Frommolt P, Wagle P, Uhlirova M. 2015. Interplay
818 among Drosophila transcription factors Ets21c, Fos and Ftz-F1 drives JNK-
819 mediated tumor malignancy. *Dis Model Mech* **8**:1279–1293.
820 doi:10.1242/dmm.020719
821 Kusch T, Florens L, Macdonald WH, Swanson SK, Glaser RL, Yates JR, Abmayr SM,
822 Washburn MP, Workman JL. 2004. Acetylation by Tip60 is required for selective
823 histone variant exchange at DNA lesions. *Science* **306**:2084–2087.
824 doi:10.1126/science.1103455
825 Lee C-H, Kiparaki M, Blanco J, Folgado V, Ji Z, Kumar A, Rimesso G, Baker NE. 2018. A
826 Regulatory Response to Ribosomal Protein Mutations Controls Translation,
827 Growth, and Cell Competition. *Dev Cell* **46**:456-469.e4.
828 doi:10.1016/j.devcel.2018.07.003

Link N, Kurtz P, O'Neal M, Garcia-Hughes G, Abrams JM. 2013. A p53 enhancer region regulates target genes through chromatin conformations in cis and in trans. *Genes Dev* **27**:2433–2438. doi:10.1101/gad.225565.113

Loubiere V, Papadopoulos GL, Szabo Q, Martinez A-M, Cavalli G. 2020. Widespread activation of developmental gene expression characterized by PRC1-dependent chromatin looping. *Sci Adv* **6**:eaax4001. doi:10.1126/sciadv.aax4001

Maraver A, Fernández-Marcos PJ, Herranz D, Muñoz-Martin M, Gomez-Lopez G, Cañamero M, Mulero F, Megías D, Sanchez-Carbayo M, Shen J, Sanchez-Cespedes M, Palomero T, Ferrando A, Serrano M. 2012. Therapeutic effect of γ-secretase inhibition in KrasG12V-driven non-small cell lung carcinoma by derepression of DUSP1 and inhibition of ERK. *Cancer Cell* **22**:222–234. doi:10.1016/j.ccr.2012.06.014

McCaffrey LM, Montalbano J, Mihai C, Macara IG. 2012. Loss of the Par3 polarity protein promotes breast tumorigenesis and metastasis. *Cancer Cell* **22**:601–614. doi:10.1016/j.ccr.2012.10.003

Muzzopappa M, Murcia L, Milán M. 2017. Feedback amplification loop drives malignant growth in epithelial tissues. *Proc Natl Acad Sci USA* **114**:E7291–E7300. doi:10.1073/pnas.1701791114

Ntziachristos P, Lim JS, Sage J, Aifantis I. 2014. From fly wings to targeted cancer therapies: a centennial for notch signaling. *Cancer Cell* **25**:318–334. doi:10.1016/j.ccr.2014.02.018

Ohsawa S, Sugimura K, Takino K, Xu T, Miyawaki A, Igaki T. 2011. Elimination of oncogenic neighbors by JNK-mediated engulfment in Drosophila. *Dev Cell* **20**:315–328. doi:10.1016/j.devcel.2011.02.007

Pagliarini RA, Xu T. 2003. A genetic screen in Drosophila for metastatic behavior. *Science* **302**:1227–1231. doi:10.1126/science.1088474

Pascual J, Jacobs J, Sansores-Garcia L, Natarajan M, Zeitlinger J, Aerts S, Halder G, Hamaratoglu F. 2017. Hippo Reprograms the Transcriptional Response to Ras Signaling. *Dev Cell* **42**:667-680.e4. doi:10.1016/j.devcel.2017.08.013

Pinal N, Martín M, Medina I, Morata G. 2018. Short-term activation of the Jun N-terminal kinase pathway in apoptosis-deficient cells of Drosophila induces tumorigenesis. *Nat Commun* **9**:1541. doi:10.1038/s41467-018-04000-6

Ranganathan P, Weaver KL, Capobianco AJ. 2011. Notch signalling in solid tumours: a little bit of everything but not all the time. *Nat Rev Cancer* **11**:338–351. doi:10.1038/nrc3035

Reddy KL, Rovani MK, Wohlwill A, Katzen A, Storti RV. 2006. The Drosophila Par domain protein I gene, Pdp1, is a regulator of larval growth, mitosis and endoreplication. *Dev Biol* **289**:100–114. doi:10.1016/j.ydbio.2005.10.042

Reinke AW, Baek J, Ashenberg O, Keating AE. 2013. Networks of bZIP protein-protein interactions diversified over a billion years of evolution. *Science* **340**:730–734. doi:10.1126/science.1233465

St Johnston D, Ahringer J. 2010. Cell polarity in eggs and epithelia: parallels and diversity. *Cell* **141**:757–774. doi:10.1016/j.cell.2010.05.011

Sykiotis GP, Bohmann D. 2008. Keap1/Nrf2 signaling regulates oxidative stress tolerance and lifespan in Drosophila. *Dev Cell* **14**:76–85. doi:10.1016/j.devcel.2007.12.002

Thurmond J, Goodman JL, Strelets VB, Attrill H, Gramates LS, Marygold SJ, Matthews BB, Millburn G, Antonazzo G, Trovisco V, Kaufman TC, Calvi BR, FlyBase Consortium. 2019. FlyBase 2.0: the next generation. *Nucleic Acids Res* **47**:D759–D765. doi:10.1093/nar/gky1003

Toedling J, Skylar O, Sklyar O, Krueger T, Fischer JJ, Sperling S, Huber W. 2007. Ringo--an R/Bioconductor package for analyzing ChIP-chip readouts. *BMC Bioinformatics* **8**:221. doi:10.1186/1471-2105-8-221

882 Toggweiler J, Willecke M, Basler K. 2016. The transcription factor Ets21C drives tumor
883 growth by cooperating with AP-1. *Sci Rep* **6**:34725. doi:10.1038/srep34725
884 Turkel N, Sahota VK, Bolden JE, Goulding KR, Doggett K, Willoughby LF, Blanco E,
885 Martin-Blanco E, Corominas M, Ellul J, Aigaki T, Richardson HE, Brumby AM.
886 2013. The BTB-zinc finger transcription factor abrupt acts as an epithelial
887 oncogene in Drosophila melanogaster through maintaining a progenitor-like cell
888 state. *PLoS Genet* **9**:e1003627. doi:10.1371/journal.pgen.1003627
889 Uhlirova M, Bohmann D. 2006. JNK- and Fos-regulated Mmp1 expression cooperates
890 with Ras to induce invasive tumors in Drosophila. *EMBO J* **25**:5294–5304.
891 doi:10.1038/sj.emboj.7601401
892 Uhlirova M, Jasper H, Bohmann D. 2005. Non-cell-autonomous induction of tissue
893 overgrowth by JNK/Ras cooperation in a Drosophila tumor model. *Proc Natl*
894 *Acad Sci USA* **102**:13123–13128. doi:10.1073/pnas.0504170102
895 Wu M, Pastor-Pareja JC, Xu T. 2010. Interaction between Ras(V12) and scribbled clones
896 induces tumour growth and invasion. *Nature* **463**:545–548.
897 doi:10.1038/nature08702
898 Xue B, Krishnamurthy K, Allred DC, Muthuswamy SK. 2013. Loss of Par3 promotes
899 breast cancer metastasis by compromising cell-cell cohesion. *Nat Cell Biol*
900 **15**:189–200. doi:10.1038/ncb2663
901 Ye J, Rawson RB, Komuro R, Chen X, Davé UP, Prywes R, Brown MS, Goldstein JL. 2000.
902 ER stress induces cleavage of membrane-bound ATF6 by the same proteases
903 that process SREBPs. *Mol Cell* **6**:1355–1364. doi:10.1016/s1097-
904 2765(00)00133-7
905
906

FIGURE LEGENDS

Figure 1. Notch-based neoplastic growth paradigms in *Drosophila* wing discs

A-D. 3rd instar wing imaginal discs at precisely 5 days after egg-laying either wild-type (WT; A), overexpressing activated Notch (N; B), mutant for *scrib* (S; C), or combining overexpressed Notch and *scrib* mutation (NS; D) and marked for E-Cad (blue) and Mmp1 (red). **A,B&D.** MARCM clones (positively marked by GFP; green) of the indicated genotypes: expressing only GFP (A; WT), expressing Nicd & GFP (B; N), and expressing Nicd & GFP and mutant for *scrib* (C; NS). **C.** Discs fully mutant for *scrib*.

E-F. Differentially expressed genes as compared to WT in the different growth paradigms N (green), S (red), and NS (blue) identified by RNA-Seq. This color code, green for N, red for S, and blue for NS is used in all figures. **E.** Heatmap of gene expressions after unsupervised clustering. **F.** Venn diagram of up-regulated and down-regulated genes in N, S, and NS.

G. Semi-quantitative RT-PCR of the indicated genes represented as fold change compared to WT (grey) in the different N (green), S (red), and NS (blue) growth paradigms and normalized to *Atc5C* expression. Biological triplicates, standard error to the mean (s.e.m.) is shown.

Figure 2. GO term analysis of the N, S, and NS transcriptomes

A. Enrichment diagram as measured by adjusted p-value for selected GO terms (full list as supplemental material) and represented as bars for N (green), S (red), and NS (blue). GO terms color reflect whether they are shared or specific: shared by all (black), common N&S (orange: mix of green and red), common N&NS (dark green: mix of green and blue), common S&NS (purple: mix of red and blue).

B. Venn diagram showing the domains of overlap of GO terms identified (significantly enriched) in N, S, and NS.

Figure 3. Polarity loss redirects the transcriptional output of Notch during neoplastic growth

A. Experimental set-up to identify the Notch Direct Targets genes (NDTs): Genes up-regulated in N, S, or NS (Transcriptomic), and located within 20kb of a Su(H) binding site (ChIP).

B. Venn diagram showing the NDTs overlap in N, S, and NS, showing core Notch responses, but also significant condition specific NDTs.
C. Overlap of the Su(H) binding sites identified by ChIP in N, S, and NS, showing that almost all S and NS Su(H) peaks are also found in N. The overlap is shown in white. Numbers are slightly different because in the Su(H) peaks calling protocol, in some rare cases, some peaks can be split between conditions where one peak in one condition would overlap with two peaks in the other.
D. Genome Viewer snapshots of several NDTs (shown in purple) such as the NS specific *Act87E* and *Wnt10* (but also *yellow-e* and *Ir87a*), the common *Ets21C*, and the N/NS NDT *upd3*. For each condition, the Su(H) ChIP enrichment is shown in the upper lane, and the Su(H) peaks identified are represented by the blocks underneath.

Figure 4. Identification of potential transcriptional modules mediating N, S, and NS growth

A. Venn diagram of significant transcription factors (TFs) identified by iRegulon as potential key mediators for the expression of the N (in the green circle), S (red circle), and NS (blue circle) up-regulated genes. Fed with lists of co-regulated genes, and analyzing the genomic features in the vicinity of the transcription start sites of these genes, iRegulon identifies potential groups of TFs and DNA-binding factors, that are enriched in the dataset of regulatory sequences, and could thus represent potential mediators of the N, S, and NS transcriptomes. TFs were color-coded according to their molecular class and/or belonging to the similar regulon (see supplemental tables S8-15). Numbers represent the number of TFs identified. See also Figure S2 for the iRegulon analyses of the NDTs, and the detailed lists of both iRegulon analyses in Supplemental tables S8 to S15.
B. Heat map for the expression of some of the transcription factors identified by iRegulon and grouped as “oncogenic module”, “basic Leucine Zippers”, “DNA damage and genome integrity”.

Figure 5. Neoplastic growth is mediated by the “oncogenic module” and by a diverse network of bZIP transcription factors including Xrp1

A-H. 3rd instar wing imaginal discs expressing *GFP*, an activated form of Notch (*Nicd*) and an RNAi for *scrib* under the control of the *Bx-Gal4* driver (dorsal wing pouch) and stained for GFP (green, white A’-H’) to assess tissue overgrowth and for

Mmp1 (red, white A''-H'') to assess tissue invasiveness. Discs also expressed under *Bx-Gal4* control the either *UAS Bsk DN* (B) or the indicated RNAi constructs: *w[HMS00045]* (A; Ctrl), *yki[KK109756]* (C), *crc[JF02007]* (D), *CG6272[HMS00057]* (E), *Xrp1[HMJ21189]* (F), *maf-S[HMS02020]* (G), *pdp1[HMS02030]* (H). Representative discs are shown.

I-K. Quantification of the overgrowth of the GFP territory in the indicated genotypes. Results are shown as percentage of discs. In blue are shown the discs smaller than the average of controls (size < Average size of controls – 1.5x StDev of controls). In green are shown discs that are the same size as the controls average or bigger. Results for the "DNA damage module" in **I**, for the "oncogenic module" in **J**, and for the "AP-1 and bZIP module" in **K**. Green arrowheads indicate modification. Star indicate a genotype with misshapen and "sick" discs. Sample size 13 – 17 discs.

For more details of RNAi lines either from the TRiP collection (labelled with trip superscript) or from the Vienna collection (labelled with KK superscript) are provided in supplemental information.

I'-K'. Quantification of the Mmp1 intensity in the indicated genotypes. Results are shown as percentage where discs were classified to fall in three categories: High Mmp1 staining intensity (red, similar to that shown in A''), Low Mmp1 staining intensity (blue, similar to that shown in C or H), No Mmp1 staining (light blue, similar to that shown in B''). Results for the "DNA damage module" in **I'**, for the "oncogenic module" in **J'**, and for the "AP-1 and bZIP module" in **K'**. Red arrowheads indicate modification. Star indicate a genotype with misshapen and "sick" discs. Sample size 13 – 17 discs.

For more details of RNAi lines either from the TRiP collection (labelled with trip superscript) or from the Vienna collection (labelled with KK superscript) are provided in supplemental information.

SUPPLEMENTAL INFORMATION

SUPPLEMENTAL MATERIAL AND METHODS

Drosophila genetics

Overexpression lines tested in the *Bx-Gal4, UAS GFP;; UAS Nicd, UAS scribHMS01490* screen were UAS GFP, UAS bskK53R [20.1a] BL#9311, and UAS SOD CAT (gift from P. Leopold). RNAi lines used are listed in the table below with an indication of the labels used in Fig. 5I-K&I'-K' and whether pictures are shown in Fig. 5A-H. TRiP collection lines have a stock BL#, and Vienna collection lines have a stock v#.

Gene	RNAi ID	Stock #	Label in Fig. 5 I-K and I'-K'	Discs shown in Fig. 5 A-H
Atf-2	HMC05118	BL#60124	Atf2 trip	
Atf3	JF02303	BL#26741	Atf3 trip	
Atf6	JF02109	BL#26211	Atf6 trip	
ATM/tefu	KK100008	v#108074	ATM KK	
ATR/mei-P26	HMC04662	BL#57268	ATR trip	
CG6272	KK110056	v#101871	CG6272 KK	
CG6272	HMS00057	BL#33652	CG6272 trip	Fig. 5E
CG7786	HMC05169	BL#62162	CG7786 trip	
cnc	HMS00650	BL#32863	cnc trip	
crc	JF02007	BL#25985	crc trip	Fig. 5D
CrebB-17A	HMJ30249	BL#63681	CrebB-17A trip	
Ets21C	HMS01989	BL#39069	Ets21C trip	
ftz-f1	KK108995	v#104463	ftz-f1 KK	
gt	HMS01105	BL#34631	gt trip	
Jra	JF01184	BL#31595	Jra trip	
kay	HMS00254	BL#33379	kay trip	
maf-S	HMS02020	BL#40853	maf-S trip	Fig. 5G
p53	HMS02286	BL#41720	p53 trip	
pdp1	HMS02030	BL#40863	pdp1 trip	Fig. 5H

Stat92E	HMS00035	BL#33637	Stat92E trip	
vri	HMS02029	BL#40862	vri trip	
w	HMS00045	BL#33644	Ctrl	Fig. 5A
Xrp1	HMS00053	BL#34521	Xrp1 trip#1	
Xrp1	HMJ21189	BL#51054	Xrp1 trip#2	Fig. 5F
Xrp1	HMJ22533	BL#60356	Xrp1 trip#3	
yki	KK109756	v#111001	yki KK	Fig. 5C

Primers

qPCR primers:

Act5C_F: GAGCGCGGTTACTCTTTCAC

Act5C_R: ACTTCTCCAACGAGGAGCTG

Act87E_F: GTCCACCGCAAGTGCTTCTA

Act87E_R: TTTCTTTGGATGGCAGGGCA

Atf3_F: CAGCATGGCAACATTGGGAC

Atf3_R: ATGAAGGCAGTGGCTGAGTC

Diap1_F: CAGCCACACGCATCTTCAAC

Diap1_R: ACTTTGTCACAGAGGAGGCG

E2f1_F: ACAGAATCCTCGCCTCCAAC

E2f1_R: GACTGCTGCCGTAGCCTATT

Ets21C_F: CTGCTCGCTGATTCGTCCAA

Ets21C_R: TAGGCATACCGCTTTCCGTG

ftz-f1_F: ATTCCTGGTCGGACATGCTT

ftz-f1_R: TTCATGCAGACATAGTCGCCC

mxc_F: ACTAGAGGAGGAGCAGCGAA

mxc_R: CTAGTGGACAGCGGCGTATT

p38a_F: TACGGACAGGTGTCAAAGGC

p38a_R: CAGCGATCCATTAGCGGGAT

p53_F: TGCGTGTGTTCCTTTGCTTC

p53_R: GTTCAGGGGGACTACAACGG

puc_F: ATTGACCTCGCCGCCAATTA

puc_R: ATTCCGCTTGAACAGAGCCA

sd_F:	AGGGTCCACAGAATGCGTTT
sd_R:	TCGCTTTCCACCTTCTCCAC
Sdr_F:	CGCTCCCTCAATCCCAAAGT
Sdr_R:	ACAACGTCCATCAGCCAGTT
Ser_F:	GCACGAATCTCTGGTGTGGA
Ser_R:	TAGATTTGGCTGGCAGTCGG
wg_F:	GCAGTCTGGTCTGGTCTACG
wg_R:	ATTGTGCGGGTTCAGTTGGA
Wnt10_F:	AATGGCATCGGTGGAACTGT
Wnt10_R:	CAGCGTCTTGCGATTGATGG

qChIP primers:

E(spl)mβ_F:	AAGTCGGAGCTTTGAATGAG
E(spl)mβ_R:	CAAGTCATTTTATTGCCCTCAC
E(spl)m5_F:	GTTTCCGCAGGTCCAGTTAC
E(spl)m5_R:	GTTTGATGTTCACGCTGCTG
white_F:	CGAAGGACGTTGACACATTG
white_R:	GAATTGCCGCTTTTTCTCAC
DDC_F:	AAGTGGGATTTGCCAGTGAC
DDC_R:	TGCTGGTGAACTTTGACTGC
CG42808_F:	CTCGTTAAGAGCAACTGCGA
CG42808_R:	GTGAGAACTCCGAATCGAGG
CG6191_F:	CGAAAAATGCGGACGATTCC
CG6191_R:	CCCACCAATCTAGGGTTTCA
Ilp8_F:	TCATCTCCGGTGTCTGACTT
Ilp8_R:	AAAGAATTGGCTGCGGAAGA

SUPPLEMENTAL FIGURE LEGENDS

Figure S1. Features of the Notch Direct Targets (NDTs) in N, S, and NS (relates to Fig. 3)

A. Genome-wide localization of the Su(H) ChIP enrichment peaks with respect to genome features, showing that the major changes were found in NS where Su(H)

"peaks" were more prevalent in introns but less prevalent at promoter regions than in N and S.

B. Heatmaps for the expression of the different NDTs in WT, N, S, and NS. From left to right are presented the N, S, NS, and finally All NDTs, highlighting that NDTs could be transcriptionally up-regulated in more than in one condition.

C. Genome browser view of the whole left arm of the 2nd chromosome, and showing the Su(H) ChIP enrichment (upper rows)) and the intervals called as Su(H) peaks (lower rows) in N (green), NS (blue), and S (red). Note the higher number of peaks in N, and the rarity of NS, or S peaks not found in N.

Figure S2. Identification of potential transcriptional modules mediating N, S, and NS growth (relates to Fig. 4)

A. Venn diagram of significant transcription factors identified by iRegulon in N, S, and NS Notch Direct Targets, and color-coded according to their molecular class. Numbers represent the number of transcription factors identified in each group. See also the detailed lists of all iRegulon analyses in Supplemental tables S8 to S15.

SUPPLEMENTAL TABLES

Table S1-3. Differentially expressed genes in N, S, and NS identified by DESeq (related to Fig. 1). Columns are:

FBgn_ID: Unique FlyBase gene ID

Symbol: Current FlyBase gene symbol

qval: adjusted p-value for multiple testing

logFC: log2 of the Fold Change "Condition N, S, or NS" / "Control WT"

Table S4. Gene Ontology (GO) enrichment in N, S, and NS (related to Fig. 2). Columns are:

experiment: type of comparison

GO_term: GO term number

description: GO term description

intersect.size: number of genes in query within the GO term

n.pw: total number of genes within the given GO term

pval: p value after hypergeometric test

qval: adjusted pvalue for multiple testing
genes: genes in query falling in the specific GO term

Table S5. Curated Gene Ontology (GO) enrichment in N, S, and NS (related to Fig. 2). Columns are:
experiment: type of comparison
GO_term: GO term number
description: GO term description
intersect.size: number of genes in query within the GO term
n.pw: total number of genes within the given GO term
pval: p value after hypergeometric test
qval: adjusted pvalue for multiple testing
genes: genes in query falling in the specific GO term

Table S6. Su(H) ChIP enrichment peaks coordinates in N, S, and NS (related to Fig. 3). Columns are:
Exp: N, S, or NS
Chr: Chromosome arm
MIN: smallest peak coordinate
MAX: biggest peak coordinate

Table S7. All Notch Direct Targets (NDTs) ordered by genomic position. This table includes an indication whether the genes are transcriptionally upregulated or have a Su(H) peak in the vicinity in each N, S, and NS condition. Columns are:
N/NS/S: NDT in the corresponding condition
Type: NDT in different conditions.
FBgn_ID: Unique FlyBase gene ID
SYMBOL: Current FlyBase gene symbol
K_ARM: Chromosome arm location of the gene
MIN (gene pos): smallest gene coordinate
MAX (gene pos): biggest gene coordinate
STRAND: +1 or -1
N Fold: Log2 Fold Change in gene expression N/WT (n.s. not significant)

N ChIP: Su(H) ChIP enrichment peak within 20kb in N (green yes, red no)
NS Fold: Log2 Fold Change in gene expression NS/WT (n.s. not significant)
NS ChIP: Su(H) ChIP enrichment peak within 20kb in NS (green yes, red no)
S Fold: Log2 Fold Change in gene expression S/WT (n.s. not significant)
S ChIP: Su(H) ChIP enrichment peak within 20kb in S (green yes, red no)

Table S8-10. iRegulon analyses of the significantly upregulated genes in N, S, and NS (related to Fig. 4). Analyses were performed using the 6K-PWM and 10kb upstream and downstream set-ups.

Table S11. Curated iRegulon analyses corresponding to Tables S8-10 (related to Fig. 4)

Table S12-14. iRegulon analyses of the Notch Direct Targets in N, S, and NS (related to Fig. S2). Analyses were performed using the 6K-PWM and 10kb upstream and downstream set-ups.

Table S15. Curated iRegulon analyses corresponding to Tables S12-14 (related to Fig. S2)

Table S16. Xrp1 target genes. Xrp1 regulated genes identified in Lee et al. (2018) (positively and negatively) and in Baillon et al. (2018). In bold are highlighted genes found in both studies. Columns are:
FBgn_ID: Unique FlyBase gene ID
Symbol: Current FlyBase gene symbol

Logeay et al. Figure 1

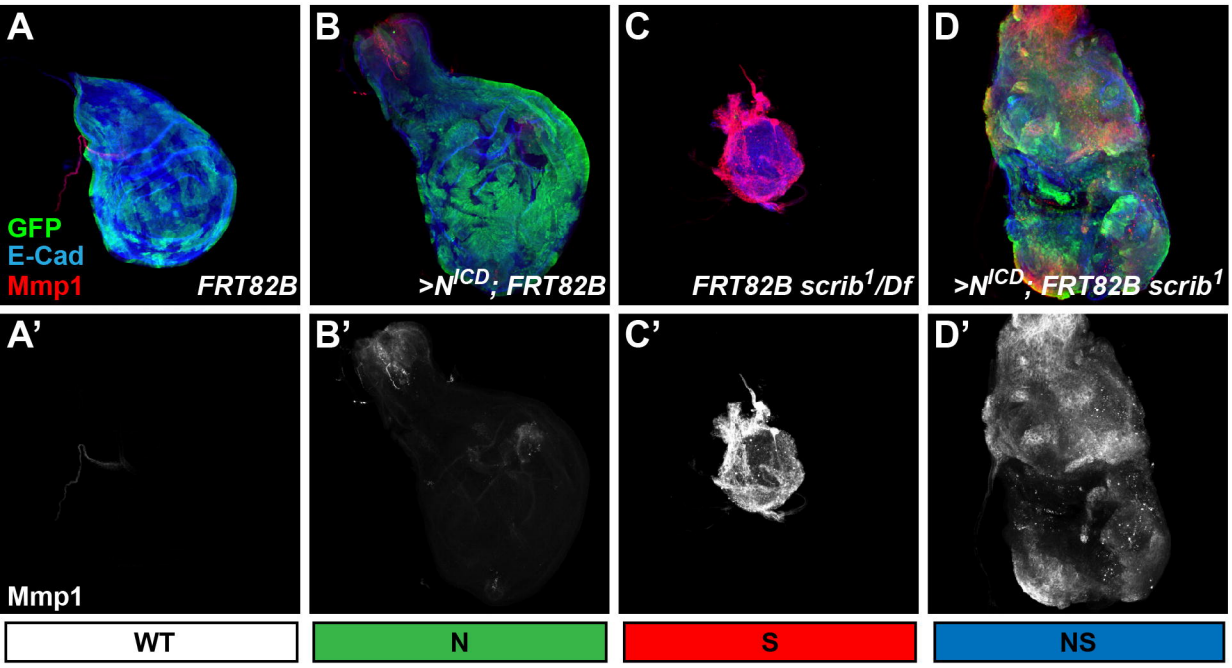

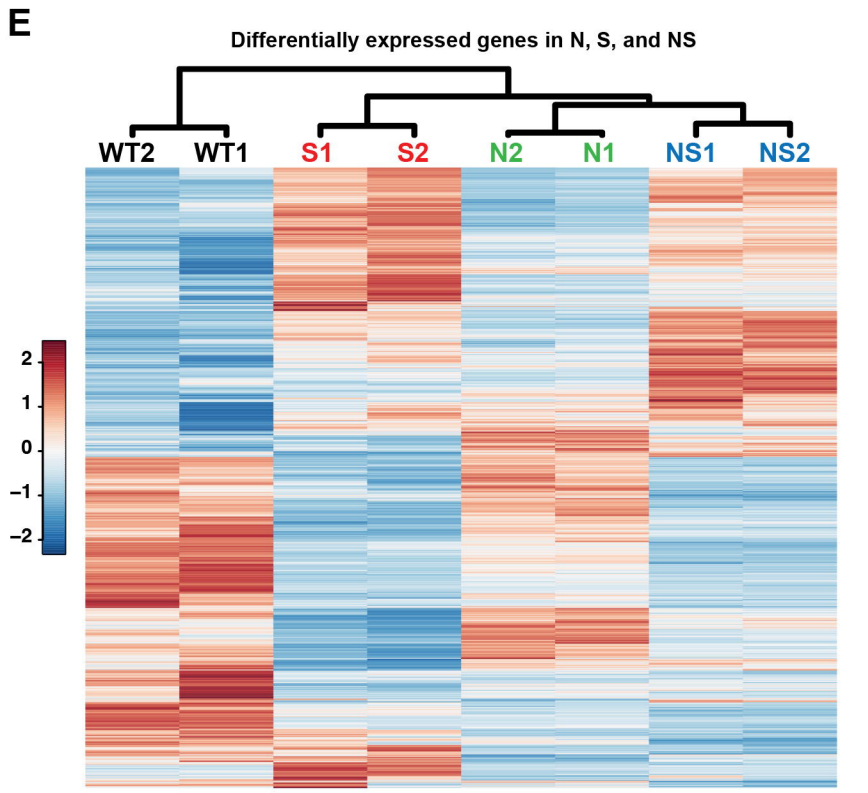

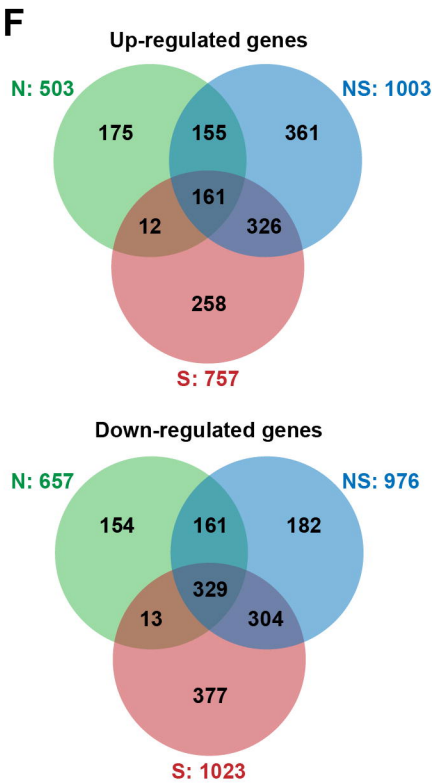

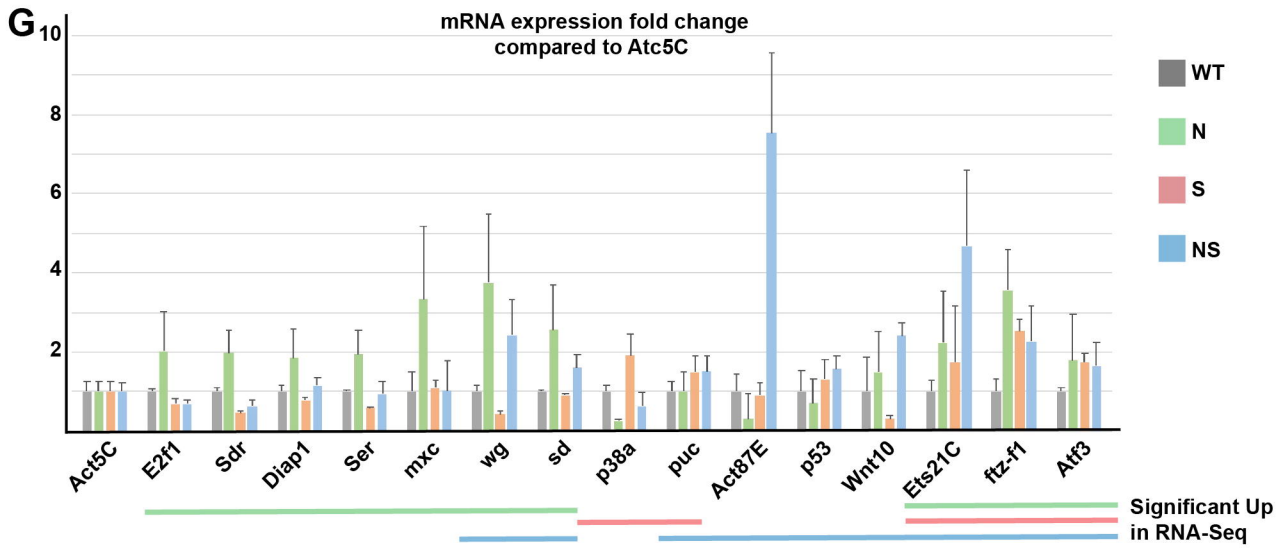

Logeay et al. Figure 2

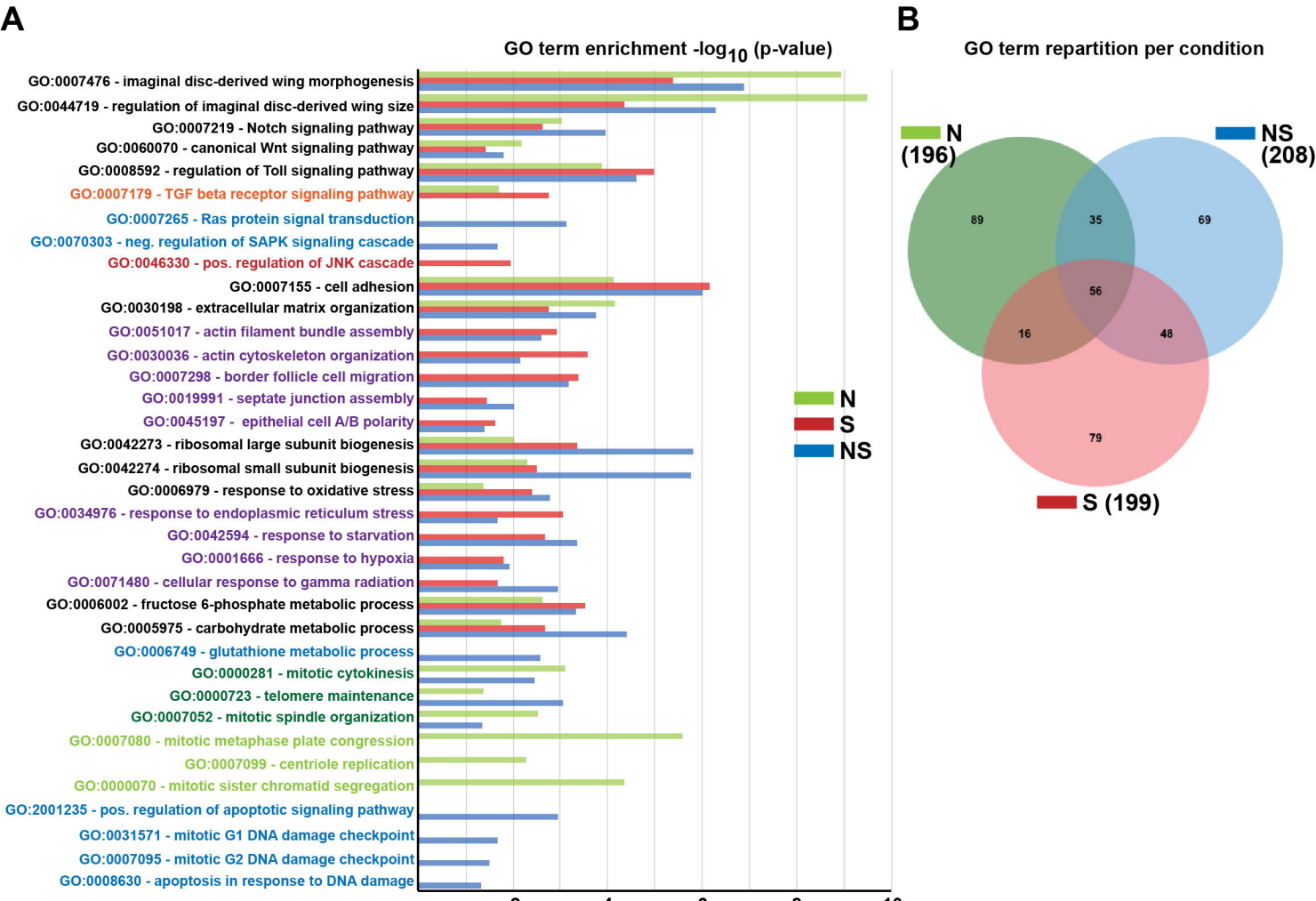

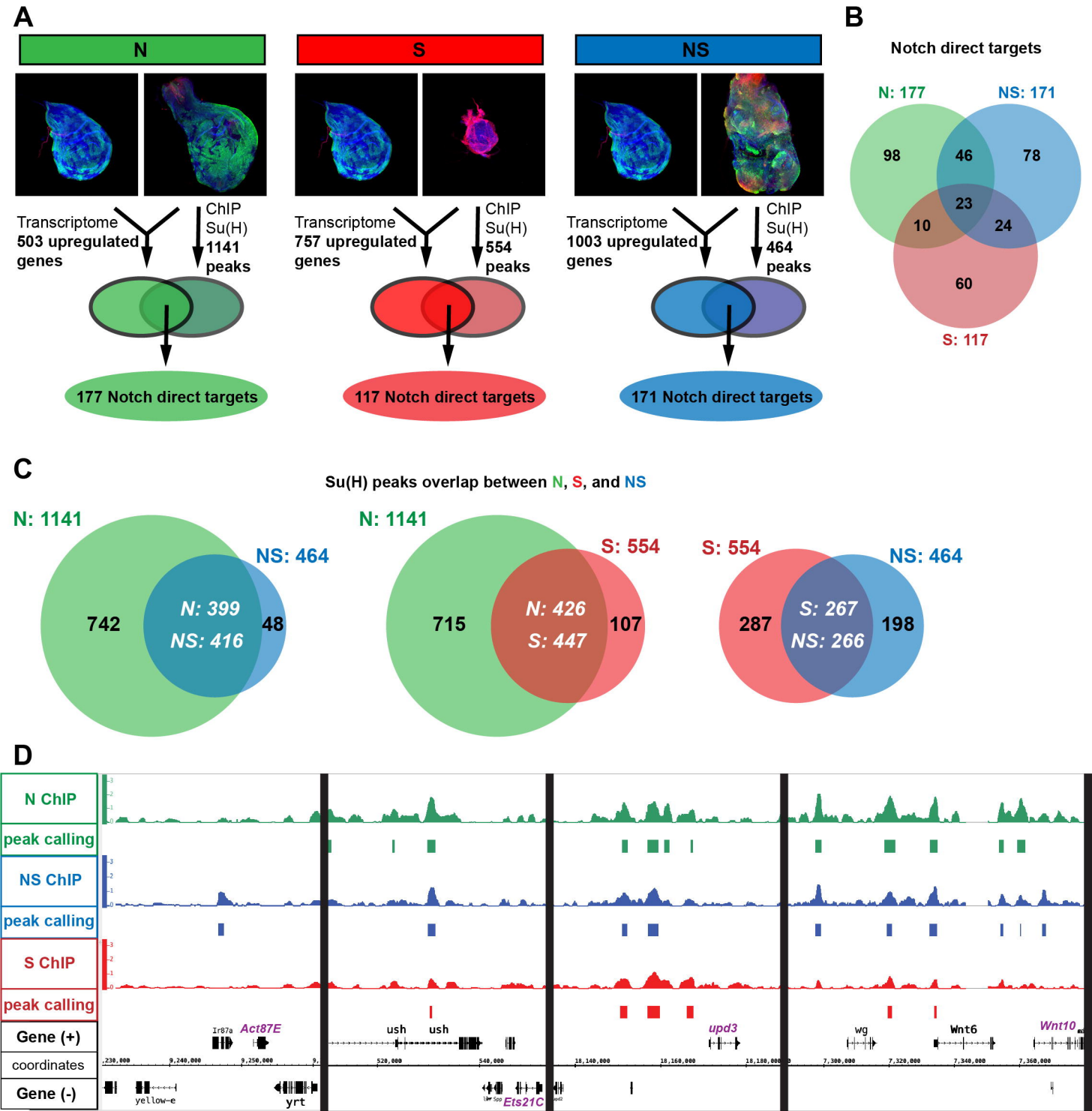
A
N
S
NS
Transcriptome
503 upregulated genes
ChIP Su(H)
1141 peaks
177 Notch direct targets
Transcriptome
757 upregulated genes
ChIP Su(H)
554 peaks
117 Notch direct targets
Transcriptome
1003 upregulated genes
ChIP Su(H)
464 peaks
171 Notch direct targets
B
Notch direct targets
N: 177
NS: 171
S: 117
98
46
78
23
10
24
60
C
Su(H) peaks overlap between N, S, and NS
N: 1141
NS: 464
742
N: 399
NS: 416
48
N: 1141
S: 554
715
N: 426
S: 447
107
S: 554
NS: 464
287
S: 267
NS: 266
198
D
N ChIP
peak calling
NS ChIP
peak calling
S ChIP
peak calling
Gene (+)
coordinates
Gene (-)
Ir87a
Act87E
ush
ush
upd3
wg
Wnt6
Wnt10
yellow-e
yrt
Ets21C

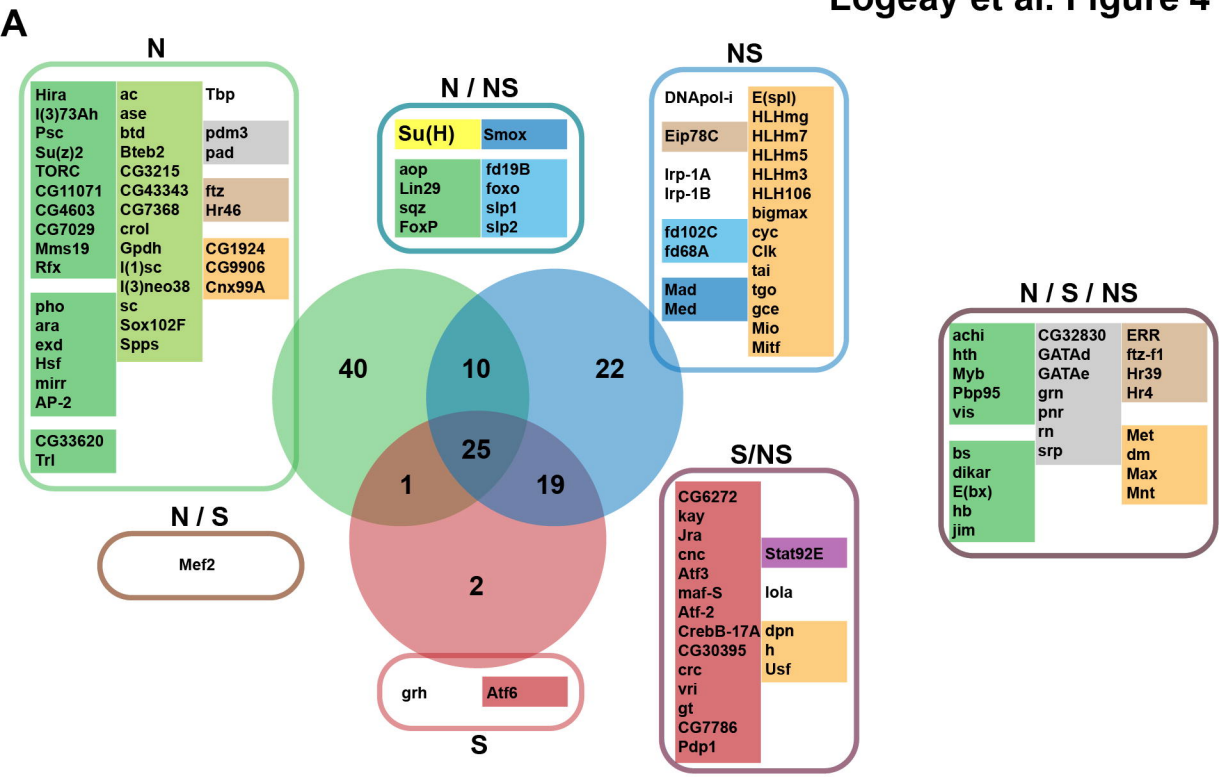
A
N
Hira
l(3)73Ah
Psc
Su(z)2
TORC
CG11071
CG4603
CG7029
Mms19
Rfx
pho
ara
exd
Hsf
mirr
AP-2
CG33620
Trl
ac
ase
btd
Bteb2
CG3215
CG43343
CG7368
crol
Gpdh
l(1)sc
l(3)neo38
sc
Sox102F
Spps
Tbp
pdm3
pad
ftz
Hr46
CG1924
CG9906
Cnx99A
N / NS
Su(H)
Smox
aop
Lin29
sqz
FoxP
fd19B
foxo
slp1
slp2
NS
DNApol-i
Eip78C
Irp-1A
Irp-1B
fd102C
fd68A
Mad
Med
E(spl)
HLHmg
HLHm7
HLHm5
HLHm3
HLH106
bigmax
cyc
Clk
tai
tgo
gce
Mio
Mitf
40
10
22
25
1
19
2
N / S
Mef2
grh
Atf6
S
S/NS
CG6272
kay
Jra
cnc
Atf3
maf-S
Atf-2
CrebB-17A
CG30395
crc
vri
gt
CG7786
Pdp1
Stat92E
lola
dpn
h
Usf
N / S / NS
achi
hth
Myb
Pbp95
vis
bs
dikar
E(bx)
hb
jim
CG32830
GATAd
GATAe
grn
pnr
rn
srp
ERR
ftz-f1
Hr39
Hr4
Met
dm
Max
Mnt
B
WT N S NS
1.5
1.0
0.5
0.0
−0.5
−1.0
bsk
ftz−fl
yki
Stat92E
Ets21C
Jra
kay
Atf−2
Atf3
crc
CG6272
Xrp1
Atf6
cnc
gt
maf−S
CG7786
vri
CrebB
Pdp1
WT N S NS
p53
mei−41
tefu
His2Av

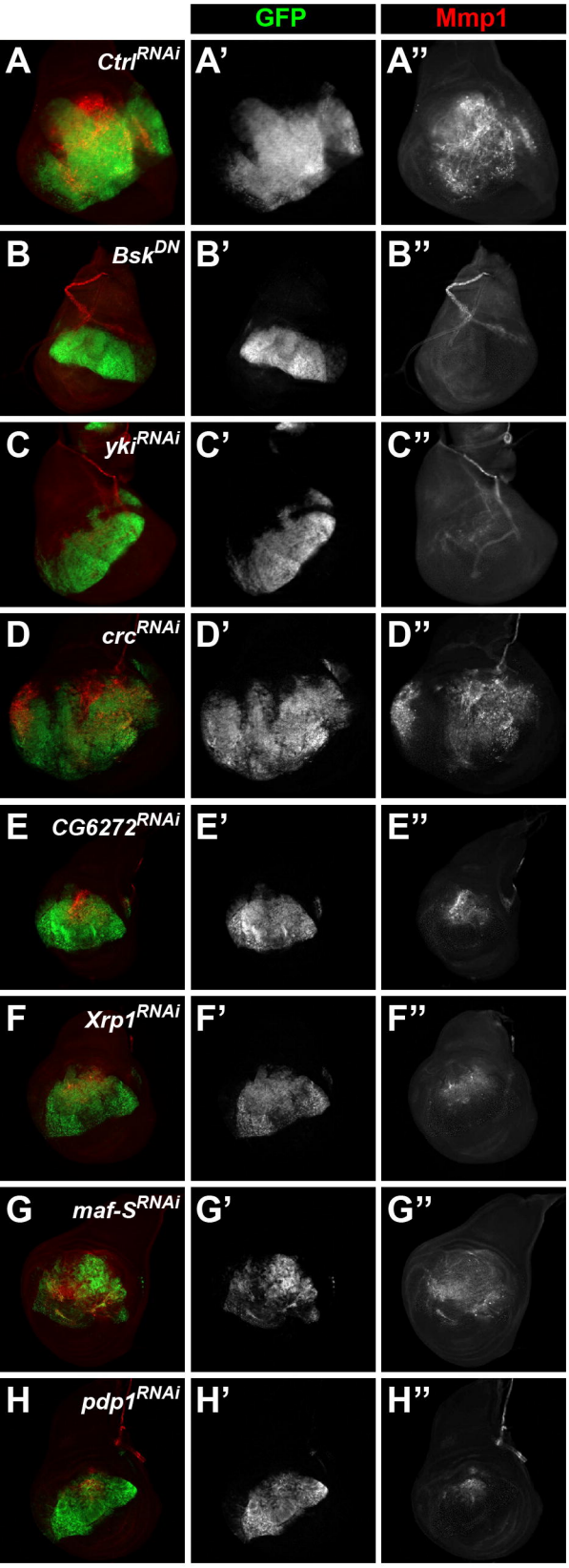
GFP
Mmp1
A Ctrl^RNAi
A' A''
B Bsk^DN
B' B''
C yki^RNAi
C' C''
D crc^RNAi
D' D''
E CG6272^RNAi
E' E''
F Xrp1^RNAi
F' F''
G maf-S^RNAi
G' G''
H pdp1^RNAi
H' H''

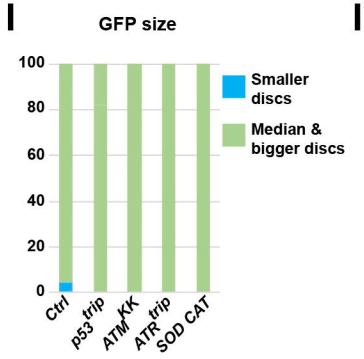
I
GFP size
Smaller discs
Median & bigger discs
Ctrl
p53 trip
ATM KK
ATR trip
SOD CAT

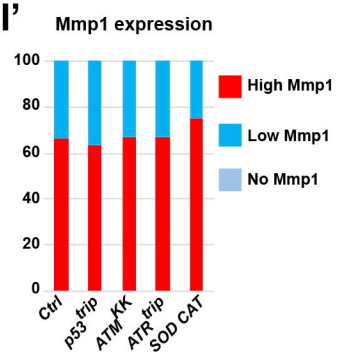
I'
Mmp1 expression
High Mmp1
Low Mmp1
No Mmp1
Ctrl
p53 trip
ATM KK
ATR trip
SOD CAT

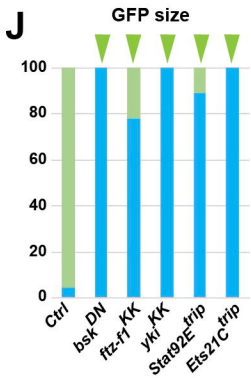
J
GFP size
Ctrl
bsk DN
ftz-f1 KK
yki KK
Stat92E trip
Ets21C trip

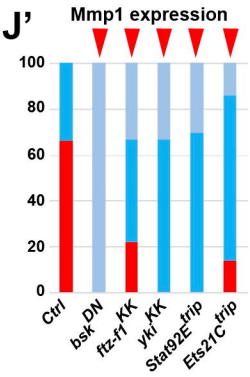
J'
Mmp1 expression
Ctrl
bsk DN
ftz-f1 KK
yki KK
Stat92E trip
Ets21C trip

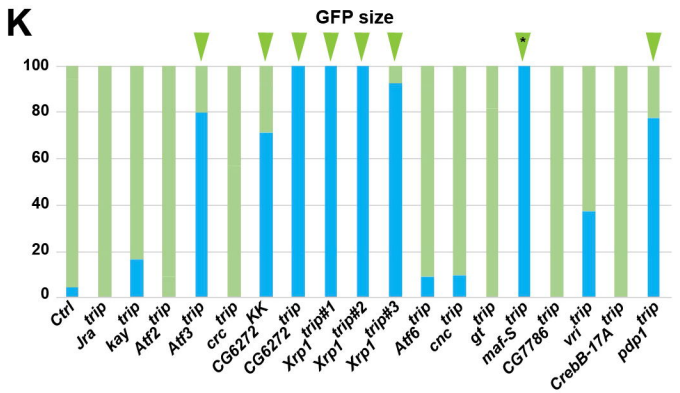
K
GFP size
Ctrl
Jra trip
kay trip
Atf2 trip
Atf3 trip
crc trip
CG6272 KK
CG6272 trip
Xrp1 trip#1
Xrp1 trip#2
Xrp1 trip#3
Atf6 trip
cnc trip
gt trip
maf-S trip
CG7786 trip
vri trip
CrebB-17A trip
pdp1 trip

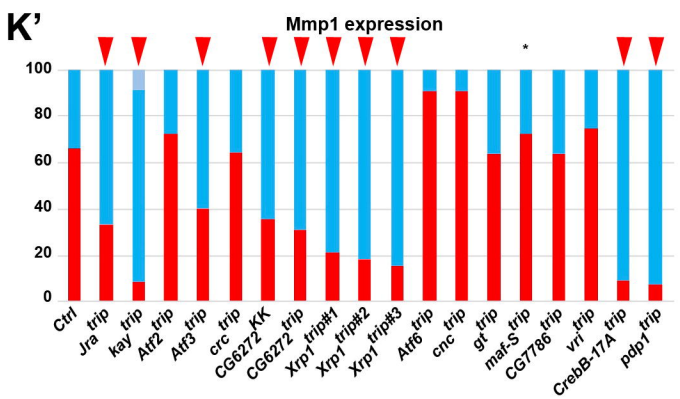
K'
Mmp1 expression
Ctrl
Jra trip
kay trip
Atf2 trip
Atf3 trip
crc trip
CG6272 KK
CG6272 trip
Xrp1 trip#1
Xrp1 trip#2
Xrp1 trip#3
Atf6 trip
cnc trip
gt trip
maf-S trip
CG7786 trip
vri trip
CrebB-17A trip
pdp1 trip

N S NS

A

Localisation of the Su(H) binding on the genome in each condition (in %)

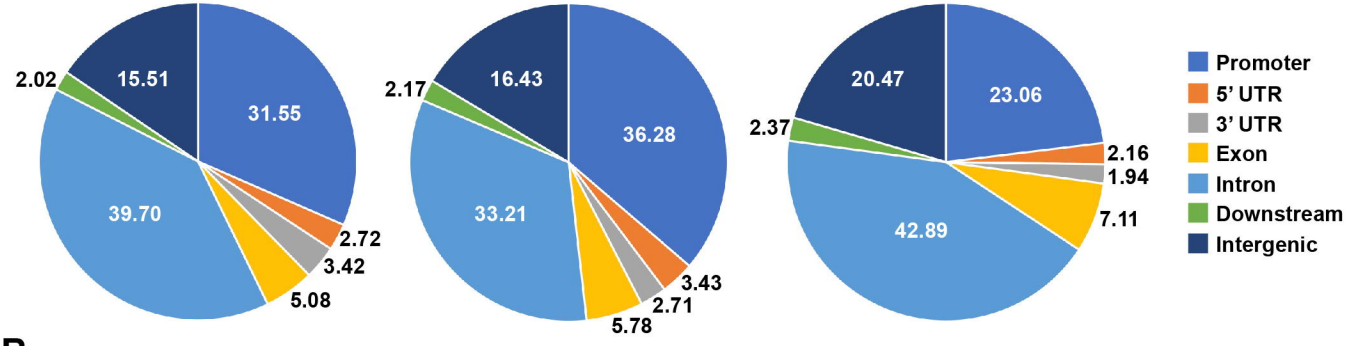

B

Heat-maps of the expression of N, S, or NS NDTs (left to right) in each condition

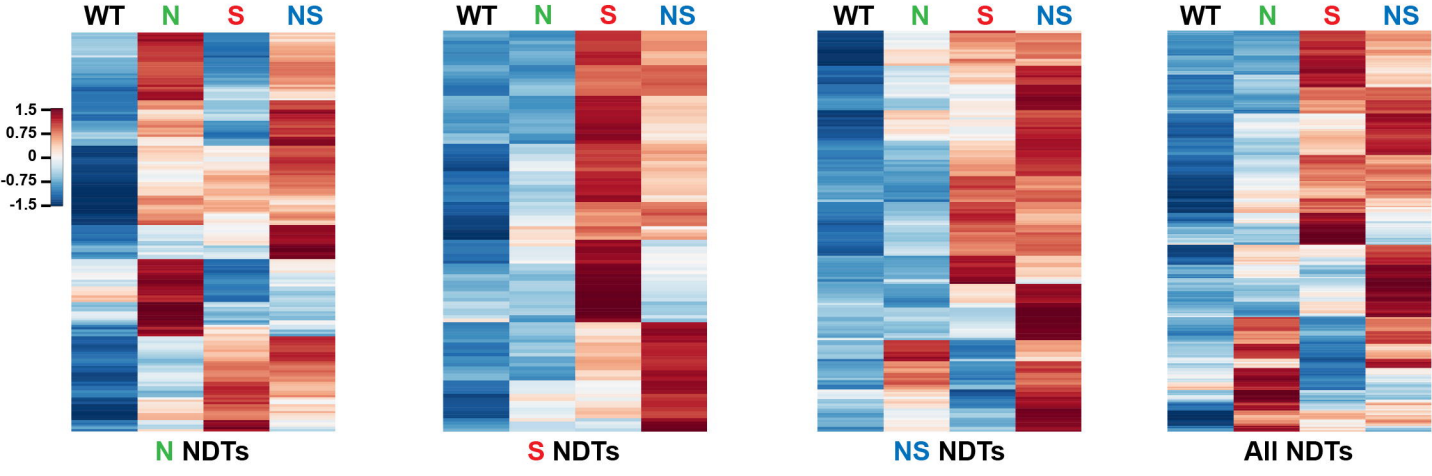

C

Genome browser view of chromosome 2L with Su(H) peak calling in N, S, and NS

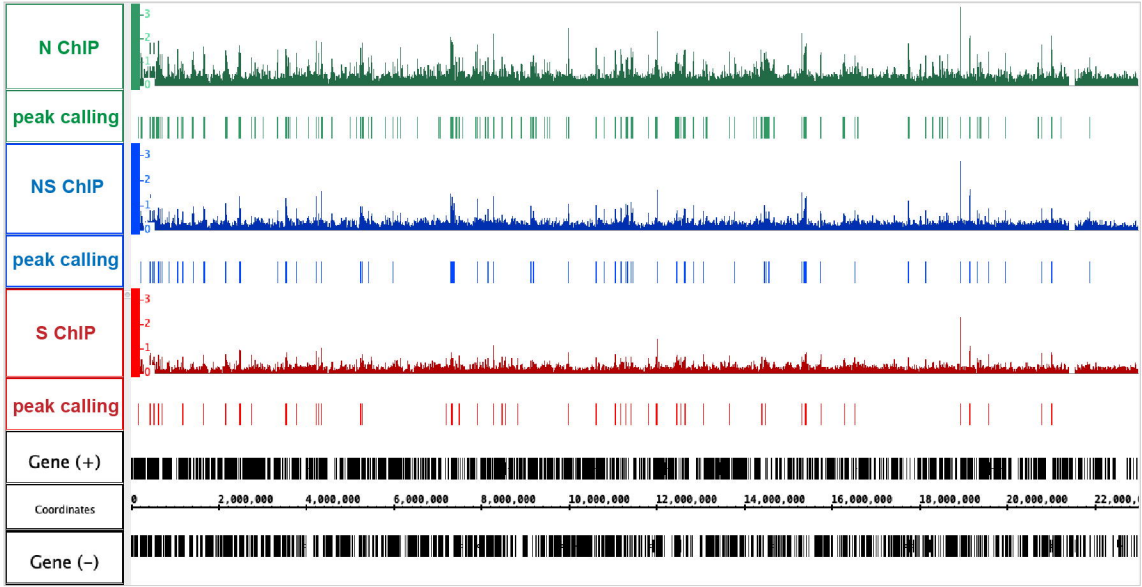

A

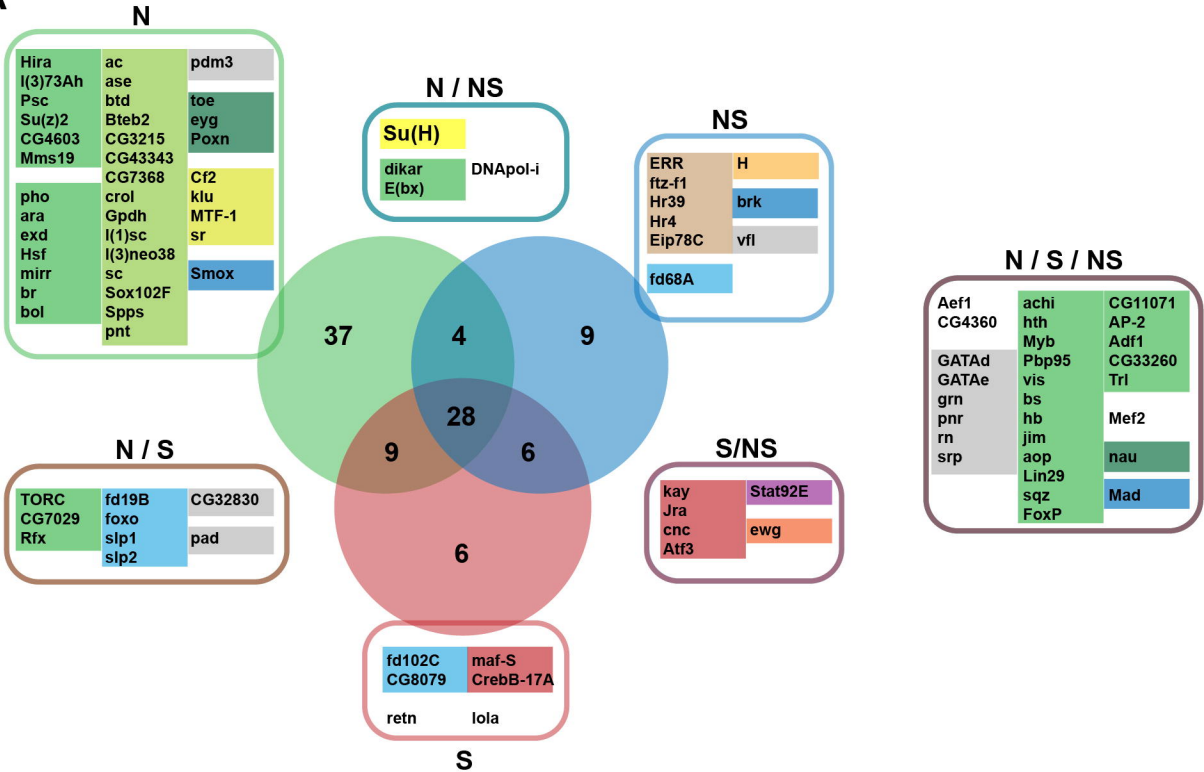
N
Hira
I(3)73Ah
Psc
Su(z)2
CG4603
Mms19
pho
ara
exd
Hsf
mirr
br
bol
ac
ase
btd
Bteb2
CG3215
CG43343
CG7368
crol
Gpdh
I(1)sc
I(3)neo38
sc
Sox102F
Spps
pnt
pdm3
toe
eyg
Poxn
Cf2
klu
MTF-1
sr
Smox
N / NS
Su(H)
dikar
E(bx)
DNApol-i
NS
ERR
ftz-f1
Hr39
Hr4
Eip78C
fd68A
H
brk
vfl
N / S / NS
Aef1
CG4360
GATAd
GATAe
grn
pnr
rn
srp
achi
hth
Myb
Pbp95
vis
bs
hb
jim
aop
Lin29
sqz
FoxP
CG11071
AP-2
Adf1
CG33260
Trl
Mef2
nau
Mad
37
4
9
28
9
6
6
N / S
TORC
CG7029
Rfx
fd19B
foxo
slp1
slp2
CG32830
pad
S/NS
kay
Jra
cnc
Atf3
Stat92E
ewg
fd102C
CG8079
maf-S
CrebB-17A
retn
lola
S